sensors

Review

Research Progress on Ammonia Sensors Based on $Ti_3C_2T_x$ MXene at Room Temperature: A Review

Kaixin Cheng [1], **Xu Tian** [1], **Shaorui Yuan** [1], **Qiuyue Feng** [1] and **Yude Wang** [1,2,*]

[1] School of Materials and Energy, Yunnan University, Kunming 650091, China; ckx0316@126.com (K.C.); xutian@mail.ynu.edu.cn (X.T.); 18787877622@163.com (S.Y.); fengqiuyue@stu.ynu.edu.cn (Q.F.)
[2] Yunnan Key Laboratory of Carbon Neutrality and Green Low-Carbon Technologies, Yunnan University, Kunming 650091, China
* Correspondence: ydwang@ynu.edu.cn

Abstract: Ammonia (NH_3) potentially harms human health, the ecosystem, industrial and agricultural production, and other fields. Therefore, the detection of NH_3 has broad prospects and important significance. $Ti_3C_2T_x$ is a common MXene material that is great for detecting NH_3 at room temperature because it has a two-dimensional layered structure, a large specific surface area, is easy to functionalize on the surface, is sensitive to gases at room temperature, and is very selective for NH_3. This review provides a detailed description of the preparation process as well as recent advances in the development of gas-sensing materials based on $Ti_3C_2T_x$ MXene for room-temperature NH_3 detection. It also analyzes the advantages and disadvantages of various preparation and synthesis methods for $Ti_3C_2T_x$ MXene's performance. Since the gas-sensitive performance of pure $Ti_3C_2T_x$ MXene regarding NH_3 can be further improved, this review discusses additional composite materials, including metal oxides, conductive polymers, and two-dimensional materials that can be used to improve the sensitivity of pure $Ti_3C_2T_x$ MXene to NH_3. Furthermore, the present state of research on the NH_3 sensitivity mechanism of $Ti_3C_2T_x$ MXene-based sensors is summarized in this study. Finally, this paper analyzes the challenges and future prospects of $Ti_3C_2T_x$ MXene-based gas-sensitive materials for room-temperature NH_3 detection.

Keywords: $Ti_3C_2T_x$ MXene; gas sensors; ammonia; room-temperature; sensitivity mechanism

Citation: Cheng, K.; Tian, X.; Yuan, S.; Feng, Q.; Wang, Y. Research Progress on Ammonia Sensors Based on $Ti_3C_2T_x$ MXene at Room Temperature: A Review. *Sensors* **2024**, *24*, 4465. https://doi.org/10.3390/s24144465

Academic Editors: Marijo Buzuk, Maša Buljac and Nives Vladislavić

Received: 27 May 2024
Revised: 7 July 2024
Accepted: 8 July 2024
Published: 10 July 2024

1. Introduction

NH_3 is a colorless, alkaline gas with a pungent odor that is now widely used in industry, agriculture, and other fields such as refrigerant and nitrogen fertilizer production. Excessive NH_3 emissions are closely related to the biological environment and the health of humans, such as the formation of acid rain and some human diseases [1,2]. According to the Occupational Safety and Health Administration (OSHA), when the human body is exposed to 35 ppm of NH_3 for more than 15 min, this will endanger human health, and when the concentration of NH_3 reaches 500 ppm, people will suffer from acute toxicity, eye pain, shortness of breath, and other symptoms, as well as the risk of asphyxiation [3,4]. In addition, NH_3 can be a marker gas for human diseases such as kidney, liver, or H. pylori infections [5], and NH_3 can be used for the early prevention of diseases and monitoring of the disease process via changes in the concentration of exhaled NH_3 in the human body [6].

A gas sensor is a sensitive device capable of converting the gas concentration that needs to be measured into an electrical signal. By analyzing the electrical signal, the sensor can obtain information such as the gas concentration present in the environment [7–9]. In recent decades, traditional commercialized NH_3 gas-sensitive materials have focused on metal oxide semiconductors (MOS) such as SnO_2, TiO_2, WO_3, ZnO, and other materials. Scientists have conducted many studies on them because they have high gas-response values [10]. However, most of the MOS-based NH_3 sensors operate at temperatures above

100 °C, and the higher operating temperature and their consumption of large amounts of energy limit their applications at room temperature and the flexible wearable applications of NH_3 [11]. Therefore, the development of a sensing material that can realize the real-time and efficient detection of NH_3, which exhibits strong sensitivity and a rapid response and can work at room temperature, is urgently needed for production safety and human health [12].

Two-dimensional (2D) transition metal carbons and nitrides (MXenes) are emerging 2D materials with a graphene-like layered structure with the general formula $M_{n+1}X_nT_x$, where the "M" stands for the early transition metals, such as Ti, V, Ta element, etc.; the "X" is the C or N element; the "n" is 1, 2, or 3; and the "T" is the surface functional group, such as hydroxyl (-OH), oxygen (-O), fluorine (-F), chlorine (-Cl), and so on [13]. MXenes were first discovered by Prof. Yury Gogotsi in 2011 [14]. Their excellent electrical conductivity, large specific surface area, and rich surface functional groups that provide more active sites for gas adsorption and reaction have attracted widespread attention and led to their use in energy storage, photovoltaic devices, supercapacitors, and gas sensors [15–17]. $Ti_3C_2T_x$ is one of the first and most extensively studied MXene materials [18]. It has been shown both theoretically and experimentally that $Ti_3C_2T_x$ MXene has excellent NH_3 sensitivity at room temperature [19]. Density functional theory (DFT) calculations have shown that the -F, -O, and -OH groups on the surface of $Ti_3C_2T_x$ MXene materials have high adsorption energies with NH_3. It was also shown that $Ti_3C_2T_x$ MXene materials are effective at sensitizing gases to NH_3 [20,21].

However, it is the high adsorption energy between $Ti_3C_2T_x$ MXene and NH_3 that also leads to the resistance drift and long recovery time from the NH_3 environment to the air. NH_3 sensors based on pure $Ti_3C_2T_x$ MXene often exhibit poor selectivity, slow response and recovery times, and low response values [22,23]. So, in order to obtain an excellent NH_3-sensitive performance at room temperature, scientists have paid a lot of attention and conducted a lot of research focused on the choice of synthesis method, composite modification, and systematic sensitization mechanism of $Ti_3C_2T_x$ MXene-based ammonia sensors.

In this context, this paper begins with $Ti_3C_2T_x$ MXene synthesis methods, provides a classified overview of the most recent research progress in $Ti_3C_2T_x$ MXene synthesis, which is primarily classified as HF etching, in situ HF etching and alkali solution etching, and summarizes the benefits and drawbacks of the various etching techniques. In addition, several types of composites, including metal–oxide semiconductors, conductive polymers, and 2D material composites, are briefly discussed in order to enhance the NH_3-sensitive behavior of NH_3 sensors based on pure $Ti_3C_2T_x$ MXene. These $Ti_3C_2T_x$ MXene composites are further analyzed to prove that the primary mechanisms of the enhanced NH_3-sensing performance of these sensors are the synergistic effects between the composites, such as the formation of a heterojunction of the composites, adsorption energy and charge transfer, chemical sensitization and electron sensitization, and the increase in specific surface area and adsorption sites due to their unique morphology [24,25].

Finally, this paper reviews the research progress regarding the sensitization mechanism of NH_3 sensors based on $Ti_3C_2T_x$ MXene, then summarizes and discusses the two current sensitization mechanisms that can explain the p-type response of MXene to either electron acceptor or electron donor gases: (1) MXene is metallic in nature, and the number of carriers decreases and the electrical resistance increases after the gas adsorption. When they exhibit semiconductor properties, the charge transfer mechanism follows the Wockenstein model [26–28]. (2) When the MXenes are exposed to the gas, the interlayer expansion hinders electron transfer and the resistance increases [16]. Finally, the paper summarizes the key challenges and potential paths forward for NH_3 sensors based on $Ti_3C_2T_x$ MXene. We expect that this review will provide novel ideas for the development of high-performance, room-temperature $Ti_3C_2T_x$ MXene NH_3 sensors.

2. Synthesis of $Ti_3C_2T_x$ MXene

The majority of $Ti_3C_2T_x$ MXene materials are produced by selectively etching the precursor MAX phase (a hexagonal layered structure with the common structural formula $M_{n+1}A_nX_n$, where the "n" = 1, 2, or 3; examples of such materials are Ti_2AlC, Ti_3AlC_2, Ti_2SiC, Ti_4AlN_3, etc.; the "A" is a group IIIA or IVA element [29,30]). The A atomic layer is more easily etched away during the reaction with the etchant, leaving a 2D layered structure with alternating M and X layers because the M-A bonds in the MAX phase are stronger than the M-X bonds in terms of bond strength.

The functional groups -OH, -O, and -F in the etching system are easily attached to the surface of this alternating layer structure, eventually forming a 2D layered structure, $Ti_3C_2T_x$ MXene [31,32]. Ti_3AlC_2 is most used in the MAX phase, as shown in Figure 1, which presents a schematic diagram of the etching process of Ti_3AlC_2 by HF, where the Ti_3AlC_2 structure consists of a single Ti_3C_2 layer separated by Al atoms. The Al atom layers between the Ti_3AlC_2 layers are eliminated by the HF treatment, and the subsequent loss of metallic bonds causes the individual Ti_3Al_2C layers to separate, producing $Ti_3C_2T_x$. The reaction process is shown in Equations (1)–(3):

$$Ti_3AlC_2 + 3HF = AlF_3 + 3/2H_2 + Ti_3C_2 \tag{1}$$

$$Ti_3C_2 + 2H_2O = Ti_3C_2(OH)_2 + H_2 \tag{2}$$

$$Ti_3C_2 + 2HF = Ti_3C_2F_2 + H_2 \tag{3}$$

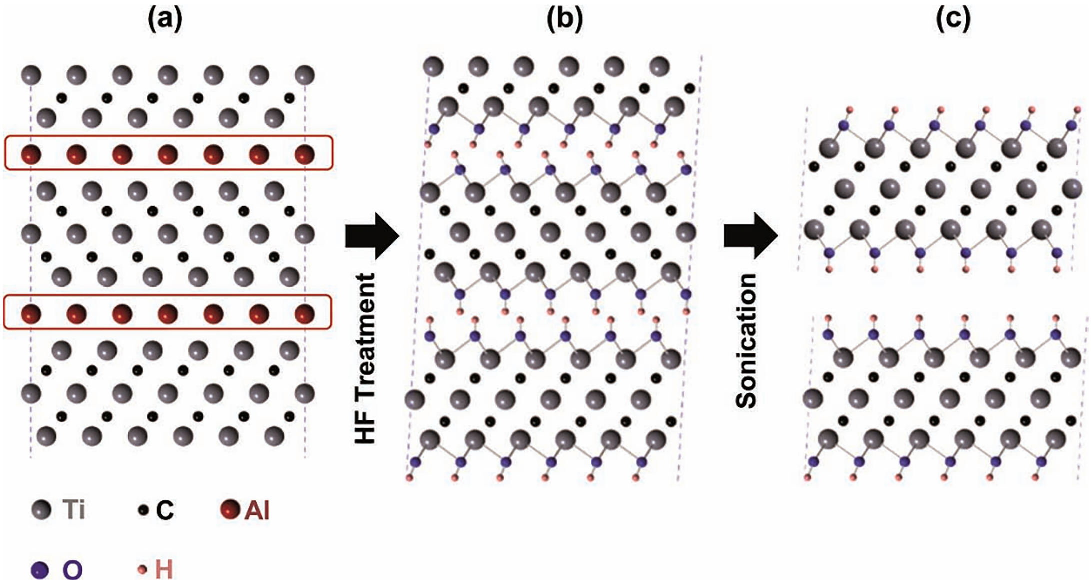

Figure 1. Ti_3AlC_2 is etched as $Ti_3C_2T_x$. (**a**) Structural schematic diagram of Ti_3AlC_2, (**b**) schematic of the process by which -OH replaces Al atoms after HF treatment, and (**c**) hydrogen bond breaking and nanolayer separation after sonication treatment [14].

The substitution of the -F functional group represented by Equation (3) is similar to that of -OH; therefore, its reaction mechanism can be considered to regard -OH in Figure 1 as -F.

The different etching methods and the choice of etchant can change the types and ratios of the functional groups at the end of the $Ti_3C_2T_x$ MXene material, thus affecting the adsorption behaviors of $Ti_3C_2T_x$ MXene and NH_3 and influencing the NH_3-sensitive performance of the sensors. In the current study, most $Ti_3C_2T_x$-based NH_3-sensing materials are synthesized using HF etching and in situ HF etching. In addition, there are a small number of research papers that mention the alkaline solution etching method. Therefore, this chapter will briefly describe these three etching methods and their effects on ammonia gas-sensing.

2.1. HF Etching

HF etching is a useful approach for preparing $Ti_3C_2T_x$ MXene, which can be created by etching the MAX phase. In 2011, Naguib et al. [14] prepared the first 2D Ti_3C_2 phase MXene by etching Ti_3AlC_2 powder with high concentrations of HF. Figure 2a shows an HFtreated SEM image of Ti_3AlC_2, revealing that the $Ti_3C_2T_x$ basal plane is accordion-like with a fan-like dispersion. The energy band structure of the synthesized MXene (Ti_3C_2) terminated with the $-OH$ and $-F$ end groups was calculated, and the results displayed that the mechanism of the electrical conductivity of the Ti_3AlC_2 material changed from metallic to semiconducting after etching due to a change in its surface chemistry (Figure 2b). Due to the simplicity of the HF etching method, it remains one of the most commonly used etchants for synthesizing $Ti_3C_2T_x$ MXene.

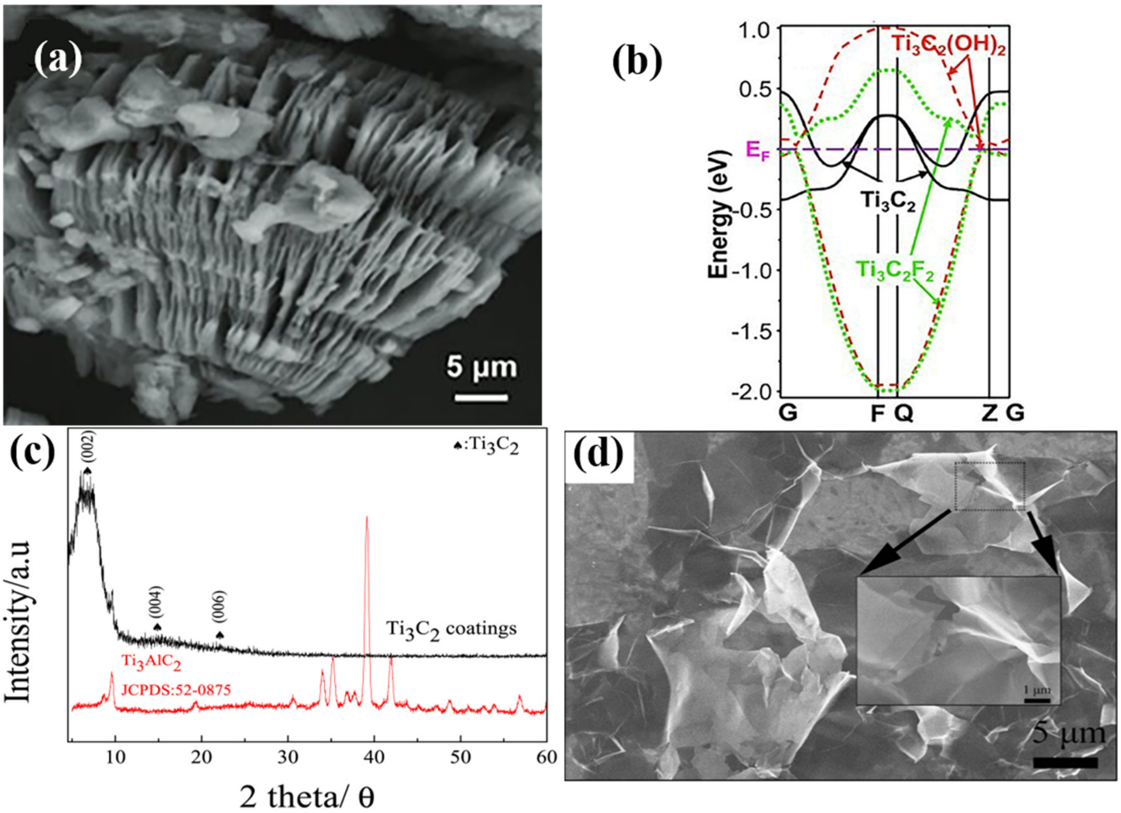

Figure 2. (**a**) SEM image of the $Ti_3C_2T_x$ MXene after HF treatment; (**b**) by comparing the single-layer band structures of $Ti_3C_2(OH)_2$, $Ti_3C_2F_2$, and Ti_3C_2, it can be seen that $Ti_3C_2T_x$ exhibits a change from metal to semiconductor due to changes in surface functional groups [14]; (**c**) XRD pattern of Ti_3AlC_2 and as-prepared $Ti_3C_2T_x$; (**d**) SEM images of Ti_3C_2 nanoflakes after exfoliation by TMAOH [33].

The specific surface area of $Ti_3C_2T_x$ MXene has a great influence on its gas-sensitive properties. The gas-sensitive properties can be improved by increasing the specific surface area of $Ti_3C_2T_x$ Mxene through intercalation and layering. For the further intercalation and delamination of $Ti_3C_2T_x$ obtained by HF etching, Lian et al. [33] reported a method involving 2D $Ti_3C_2T_x$ nanosheets synthesized by intercalation and a delamination reaction in tetramethylammonium hydroxide (TMAOH) solution after dilute HF etching. They added a quantitative amount of Ti_3AlC_2 powder to a 5% concentrated HF solution, which was magnetically stirred at room temperature for 24 h. Then, the suspension was washed with deionized water until the pH of the supernatant was 5–6 and centrifuged. After that, the precipitate was put in a 25% solution of tetramethyl hydroxide (TMAOH) and magnetically agitated for another 24 h to allow for more intercalation and delamination. Afterward, the precipitate was centrifuged to obtain the two-dimensional, less-layered $Ti_3C_2T_x$ nanosheets. Figure 2c displays the XRD spectra of Ti_3AlC_2 and Ti_3C_2. After HF etching, the (104) diffraction peak of Ti_3AlC_2 at $2\theta \approx 39.1^\circ$ almost disappeared, which indicated that the Ti_3C_2 was completely stripped [34,35]. The SEM image of the Ti_3C_2 nanoflakes intercalated with TMAOH is shown in Figure 2d. A high level of delamination is indicated by the two-dimensional structure, semi-transparent, and wrinkled textures of the Ti_3C_2 nanoflakes. In future research, we can increase the specific surface area of $Ti_3C_2T_x$ MXene-sensitive materials through the intercalation and delamination of $Ti_3C_2T_x$ to increase the adsorption sites on the surface of the materials to promote their adsorption and gas reaction with ammonia molecules, ultimately aiming to achieve the purpose of improving the sensitivity of $Ti_3C_2T_x$ MXene.

2.2. In-Situ HF Etching

Although the HF etching process is easy to operate, it has obvious disadvantages, such as a longer etching time and a more dangerous operation [36]. Furthermore, the $Ti_3C_2T_x$ MXene obtained by this process has more shortcomings: HF is dangerous to humans and the environment, and fluorine-containing functional groups are inert, degrading their properties. In 2014, Ghidiu et al. [37] presented a method to synthesize $Ti_3C_2T_x$ MXene by etching the Ti_3AlC_2 phase in situ with LiF and HCl solution. Specifically, LiF was added to a 6 M HCl solution and stirred to dissolve before slowly adding Ti_3AlC_2 powder and maintaining this at 40 °C for 45 h. After that, the mixture was washed until the pH of the supernatant was 6. The obtained deposit formed a clay-like paste, which was rolled between the roller mill's permeable membranes to produce pliable, freestanding thin films within a few minutes. When diluted, it can be applied as an ink to deposit or print MXene on various substrates.

During the reaction process, Li^+ can spontaneously insert into the interlayer of $Ti_3C_2T_x$ MXene, and due to the hydrophilicity of $Ti_3C_2T_x$ MXene, water molecules can easily enter the interlayer, leading to a much larger lattice parameter for $Ti_3C_2T_x$ MXenes obtained by LiF/HCl etching than for $Ti_3C_2T_x$ MXenes obtained by HF etching. This process produces large-component monolayer $Ti_3C_2T_x$ flakes with a high yield, large lateral size, and excellent quality. More importantly, using LiF and HCl to etch MAX avoids the use of concentrated HF, which is very corrosive and poisonous, while also reducing the nanoscale defects generated by direct etching with HF. Furthermore, the simplicity of this method contrasts with previous films produced through laborious insertion, layering, and filtration techniques [38]. It is noteworthy that MXenes can still be obtained when H_2SO_4 is used instead of HCl. However, fine-tuning the etching reagent might affect the surface chemistry or the intercalation ions, which needs more exploration. Currently, in situ etching by LiF and HCl solutions is widely used in the synthesis of $Ti_3C_2T_x$ MXene materials.

Han et al. [39] compared the ammonia sensitivity of $Ti_3C_2T_x$ MXene materials synthesized by HF etching and LiF/HCl etching. They found that the $Ti_3C_2T_x$ materials prepared by the LiF/HCl etchant had better gas sensitivity than that of HF etchant. They could detect a wide range of NH_3 at room temperature with higher sensitivity and stability. The higher sensing performance of the $Ti_3C_2T_x$ MXene materials obtained by the LiF/HCl etching method was analyzed to be due to the high ratio of -O and -OH functional groups on the surface of $Ti_3C_2T_x$ materials prepared by this method.

2.3. Alkali Solution Etching

Yang et al. [40] improved the humidity and NH_3-sensing properties of organ-like $Ti_3C_2T_x$ MXene synthesized from HF solution via alkalization. Organ-like $Ti_3C_2T_x$ MXene is a class of $Ti_3C_2T_x$ MXene materials that can provide a fast pathway for charge and ion transfer, thereby preventing the reduction in specific surface area due to the restacking of layers. Firstly, $Ti_3C_2T_x$ MXene powder was prepared through HF acid etching using Ti_3AlC_2 and a 45 wt% HF solution. Subsequently, the obtained $Ti_3C_2T_x$ MXene powder was put into a 5 M NaOH solution and subjected to continuous magnetic stirring at room temperature for 2 h, and the alkalized $Ti_3C_2T_x$ powder was finally obtained. The alkali treatment embeds Na^+ in the interlayer of $Ti_3C_2T_x$, which plays a crucial role in regulating water for humidity sensing. During stage 1 of Figure 3, several water molecules are coupled with a single Na^+ ion, forming a stable $[Na(H_2O)_m]^+$ cluster structure. Meanwhile, in stage 2 of Figure 3, the alkaline treatment enhances the N-Ti bonding sites due to the increased -O terminus, resulting in higher NH_3 adsorption. The alkalized $Ti_3C_2T_x$ devices have an improved sensing performance for humidity and NH_3 compared to non-alkalized $Ti_3C_2T_x$, due to the embedding of Na^+ and the higher oxygen-to-fluorine atomic number ratio ([O]/[F]), and have the opposite response signal.

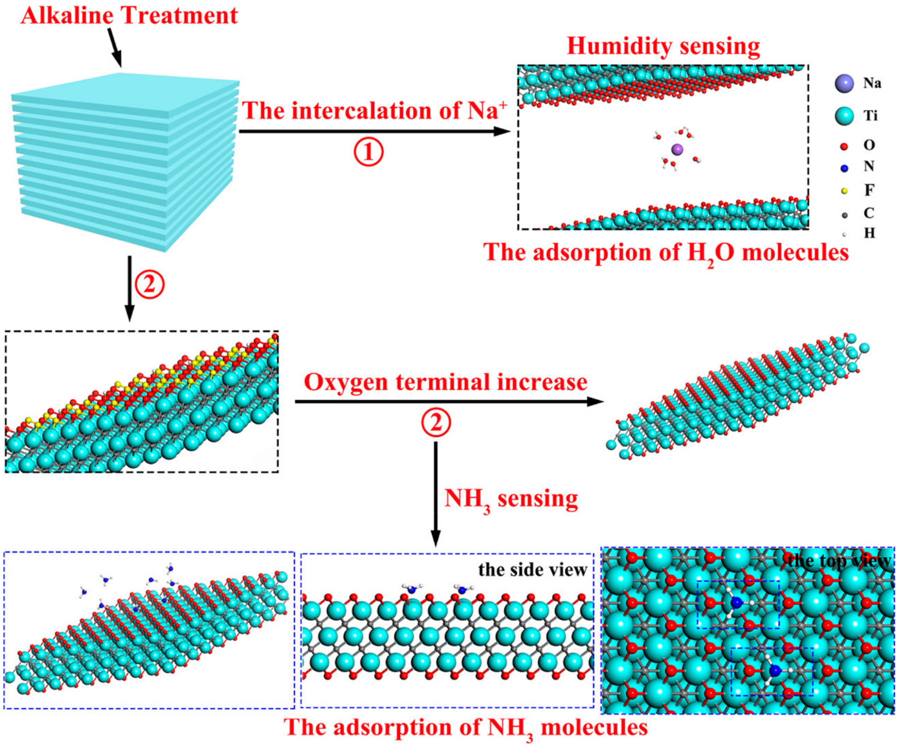

Figure 3. Adsorption process of H_2O and NH_3 molecules on the surface of alkalized $Ti_3C_2T_x$ [40].

Although there is no report on the synthesis of $Ti_3C_2T_x$ MXene ammonia-sensitive materials using only alkali etching, this method allows for the preparation of $Ti_3C_2T_x$ MXene with a large number of oxygen-containing functional groups, is simple to perform, and does not contain inert groups -F. Therefore, it is expected to be applicable to the synthesis of $Ti_3C_2T_x$ MXene-based ammonia-sensitive materials in the future and to obtain sensitive materials with a strong ammonia-adsorption capacity.

$Ti_3C_2T_x$ MXene synthesized by conventional fluoride-containing methods usually uses fluoride ion-containing solutions as an etchant, which is harmful to the environment. In addition, highly reactive fluoride ions can penetrate into the human body and cause fatal damage to body tissues [41,42]. It has been demonstrated that fluoride-based etching procedures generate a large number of -F-terminal functional groups [43,44], which substantially limit charge transfer and diminish chemically active sites, hence compromising the electrochemical characteristics of $Ti_3C_2T_x$ MXene [45–47]. Therefore, modulating the terminal functional groups of $Ti_3C_2T_x$ MXene can affect its electrochemical properties and NH_3 sensitivity [48]. Furthermore, the popular HF and LiF/HCl etching methods are typically time-consuming [49]. Therefore, it is important to develop environmentally friendly and F-free synthesis routes for NH_3 sensor-based $Ti_3C_2T_x$ MXene in the future.

3. $Ti_3C_2T_x$ MXene-Based Nanocomposites Material Gas Sensors for NH_3

$Ti_3C_2T_x$ Mxenes are a typical new 2D material with high selectivity for ammonia at room temperature. Dillon, Lipatov et al. [35,50] measured the high electrical conductivity of $Ti_3C_2T_x$ MXene to be 6500 S cm^{-1} and 4600 ± 1100 S cm^{-1}. Halim et al. [51] have also reported that Ti_3C_2 films exhibit metal conductivity at a temperature of about 100 K. $Ti_3C_2T_x$ MXenes is considered to have good application prospects for ammonia detection at room temperature due to its excellent electrical conductivity, unique structure, and the large number of adsorption sites provided by functional groups such as -O and -OH on the surface [52–54]. Due to the low response values, serious base-resistance drift, and poor stability of pure $Ti_3C_2T_x$ MXenes when utilized as ammonia-sensing materials, it is essential to combine $Ti_3C_2T_x$ MXene with other sensitive materials to enhance their sensing capabilities [25,55,56]. In this chapter, a brief overview will be provided of the most-researched methods of compositing several sensitive materials with $Ti_3C_2T_x$ MXenes to improve their sensing performance. These methods include combining them with MOS materials, conductive polymer materials, and certain 2D materials.

3.1. Metal Oxide Modification

MOS materials such as TiO_2, SnO_2, In_2O_3, WO_3, and $Ti_3C_2T_x$ MXene usually use synergistic effects such as the Fermi energy level effect (Fermi level bending, carrier separation, depletion layer regulation, and increase in interfacial barrier energy) between the composites, the formation of heterojunctions, and the specific morphology, etc., to enhance the gas-sensitive performance of the sensors [57–59]. In particular, for $TiO_2/Ti_3C_2T_x$ MXene nanocomposites, in addition to the introduction of TiO_2 material in the matrix, due to the instability of $Ti_3C_2T_x$ MXene, TiO_2can be synthesized through partial oxidization to $Ti_3C_2T_x$ MXene, leading to in situ derivatization using techniques such as high-temperature sintering.

When a semiconductor material is irradiated by UV light whose optical energy is larger than its band gap, photocarrier pairs are generated at the interface of the sensitive material [60,61], and the additionally generated photogenerated electrons and holes can promote the adsorption and desorption processes and redox reactions of gases, thus improving the response value and shortening the response recovery time of the sensor [62,63]. Therefore, using the UV irradiation of gas sensors to obtain highly NH_3-sensitive $Ti_3C_2T_x$ MXene-based sensors operating at room temperature is a feasible strategy.

To overcome the limitations of $Ti_3C_2T_x$ MXene as a room-temperature ammonia gas sensor, such as limited its sensitivity and selectivity, Zhang et al. [64] proposed growing TiO_2 on $Ti_3C_2T_x$ MXene in situ. They also utilized UV light (the light energy of the used 365 nm UV light source is 3.4 eV, which is larger than the band gap 1.6 eV of (001)$TiO_2/Ti_3C_2T_x$) to boost the performance of the (001) TiO_2/MXene heterostructure ammonia gas sensor. The $Ti_3C_2T_x$ powder was prepared by removing the Al layer from MAX (Ti_3AlC_2) with a 50% HF solution. $NaBF_4$ (0.1 mol/L, 8 mL) was introduced as a control agent for the crystal surface in the HCl solution of $Ti_3C_2T_x$. The mixture was then hydrothermally treated at 160 °C for 8, 12, 16, and 32 h. The hydrothermal reaction promoted the formation of (001) planes during the crystal growth process, converting Ti in Ti_3C_2 into hydrated Ti_3^+ ions and binding F ions to the (001) planes with the aid of $NaBF_4$ as an inducer. As shown in Figure 4a, the T-T-12 h TiO_2/MXene sensor that undergoes a hydrothermal reaction for 12 h is more sensitive to ammonia, with a lower detection limit than that of the pure $Ti_3C_2T_x$-based sensor, and also exhibits good durability in terms of its response/recovery time, repeatability, and selectivity. Analyzing the energy band diagram schematic of the T-T-12 h TiO_2/MXene-based sensor demonstrated in Figure 4c, it can be concluded that the enhanced gas-sensitive performance of NH_3 is obtained because $Ti_3C_2T_x$ greatly facilitates the separation of electron–hole pairs by storing holes through the Schottky junctions formed at the interfaces with TiO_2, which enhances the ammonia-sensing performance. In Figure 4d, we can see that adding UV light to the highly active (001) crystalline TiO_2 makes the charge separation of the T-T-12 h TiO_2/MXene sensor when exposed to UV light even better, which leads to a better gas-sensing performance. Figure 4b also shows a two-fold increase in sensitivity compared to when UV is absent. The TiO_2/MXene sensor type T-T-12 h exhibited 34 times more sensitivity to 30 ppm of ammonia compared to pristine $Ti_3C_2T_x$. Density functional theory reveals that the (001) side of the TiO_2 and $Ti_3C_2T_x$ composite has the greatest attraction in terms of ammonia adsorption [64].

To further improve the sensing performance of pure $Ti_3C_2T_x$ MXene for NH_3, Kan et al. [65] combined surface-functionalized In_2O_3 nanotubes with $Ti_3C_2T_x$ nanosheets. The composite was further loaded onto thermoplastic polyurethane (TPU) foam, a dual-functional sensing platform constructed based on $Ti_3C_2T_x/In_2O_3$ nanocompositesand modified TPU foam sensors. The produced nanocomposites exhibited an improved ammonia-sensing performance and pressure-sensitive properties, utilizing the strong synergistic effect of the sensing of In_2O_3 nanotubes and high conductivity of $Ti_3C_2T_x$ nanoflakes, as well as the foam substrate's pressure-sensitive and gas-permeable capabilities. $Ti_3C_2T_x$ nanoflakes are negatively charged on the surface due to the terminal functional groups such as -OH and -F. At this time, the modification of In_2O_3 with the cationic surfactant (3-aminopropyl) triethoxysilane (APTES) can make the surface of In_2O_3 positively charged, and the two can be compounded to obtain $Ti_3C_2T_x/In_2O_3$ composites via simple ultrasonication with electrostatic adsorption, which was shown to have higher NH_3 response values than pure $Ti_3C_2T_x$ nanoflakes. In_2O_3 is an n-type sensing material, which has a bandgap in the range of 3.55–3.75 eV [66] and a work function of about 4.28 eV [67]; $Ti_3C_2T_x$ MXene behaves as a p-type sensing material, which has a bandgap of 0.19 eV [68] and a work function of about 4.5 eV [69]. Two main factors are used to investigate the enhanced sensing ability: First, n-type In_2O_3 has a high Fermi energy level, and electrons will be transferred from the In_2O_3 nanotubes to the $Ti_3C_2T_x$ nanoflakes until the Fermi energy levels of the two reach equilibrium, thus forming a space charge layer at the $Ti_3C_2T_x$ and In_2O_3 interface. At the same time, the energy bands at the interface are bent on both sides, generating a potential barrier that increases the base value resistance of the sensor, thus increasing the gas response. Second, the In_2O_3 nanotubes work as isolators to inhibit the re-stacking of $Ti_3C_2T_x$ nanoflakes, thereby increasing the layer space and effectively facilitating the diffusion and permeation of gases in the sensing layer. In addition, the sensor achieves the flexible and interference-free detection of complex exhaled environments at room temperature, with a memory function for detecting NH_3 gases down to 1 ppm, realizing the dual-mode detection of NH_3 gases.

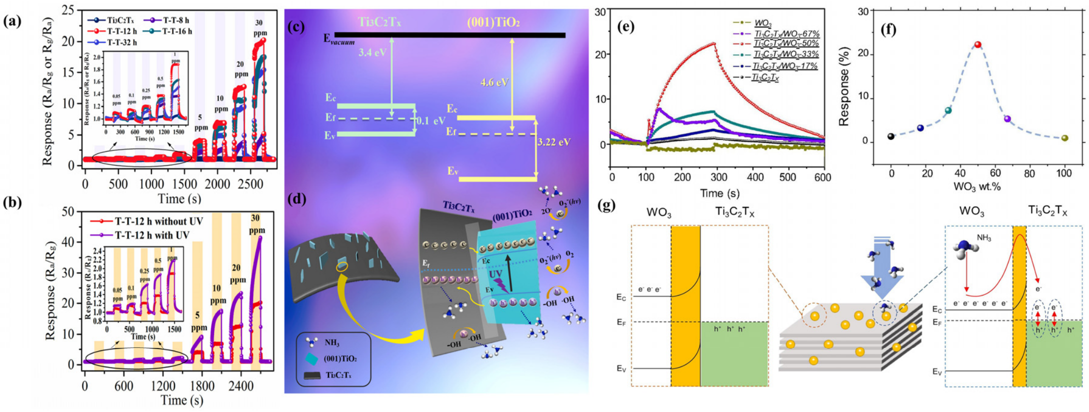

Figure 4. (**a**) Dynamic response curves of TT8 h-, TT12 h-, TT16 h- and TT32 h-based sensors; (**b**) dynamic response curves with UV illumination on T-T-12 h and without UV illumination on TT12 h; (**c**) schematic illustration of band diagrams of $Ti_3C_2T_x$ and (001) TiO_2; (**d**) schematic illustration of ammonia gas-sensing mechanism under UV irradiation [64]. (**e**) The transient response curves of the composite sensors with different WO_3 contents to 1 ppm NH_3 at room temperature; (**f**) the dependence of the composite sensor response on the WO_3 content; (**g**) schematic illustration of the gas-sensing mechanism and the energy band structure diagram of $Ti_3C_2T_x/WO_3$ before and after exposed NH_3 [70].

To address the limited sensitivity of $Ti_3C_2T_x$ MXene gas sensors, Guo et al. [70] reported a $Ti_3C_2T_x/WO_3$ composite resistive sensor that had excellent NH_3 sensitivity at room temperature. $Ti_3C_2T_x/WO_3$ composites with WO_3 nanoparticles anchored on $Ti_3C_2T_x$ nanosheets were prepared using an ultrasonic technique. As demonstrated in Figure 4e,f, the detection sensitivity of the $Ti_3C_2T_x/WO_3$-50% sensor was up to 22.3%, which was 15.4 times higher than that of the pure $Ti_3C_2T_x$ sensor, at 1 ppm NH_3 at room temperature. The improved NH_3-sensing performance is mainly attributed to the increase in the aspect ratio of the composite, the increase in the active sites provided by WO_3, and the more effective charge transfer bestowed by the formed heterojunction (Figure 4g). It was demonstrated that the $Ti_3C_2T_x/WO_3$-50% sensor remained effective over a wide range of relative humidity (RH) conditions (3.5%~72.9% RH), and low concentrations of NH_3 were still detected even at high humidity. As RH increases, the sensor response to NH_3 sensing gradually decreases. Humidity compensation methods, which are often used in practical applications, can help to solve the humidity effect's limitations.

Table 1 outlines the gas-sensitive properties of different MOS/$Ti_3C_2T_x$ MXene composites towards NH_3 at room temperature in recent years. The acronym "LOD" in the table refers to "the limit of detection".

Table 1. The gas-sensitive properties of various MOS/$Ti_3C_2T_x$ MXene nanocomposites to NH_3 at room temperature.

Materials	**Concentration (ppm)**	**Response Value (R_a/R_g, R_g/R_a) or Response Rate [($\Delta R/R_g$) × 100%]**	**LoD**	**Response/Recovery Time (s)**	**Ref./Year**
$NiO/Ti_3C_2T_x$	50	6.13	10 ppm	60/19	[71]/2023
$Ti_3C_2T_x/In_2O_3$	30	63.8%	2 ppm	42/209	[57]/2022
$TiO_2/Ti_3C_2T_x$	10	3.1%	0.5 ppm	33/277	[22]/2019
$Ti_3C_2T_x/WO_3$	1	22.3%	1 ppm	119/228	[70]/2021
$Ti_3C_2T_x/CuO$	5	46.7%	5 ppm	12/25	[72]/2023
$ZnO/Ti_3C_2T_x$	20	39.16%	89.41 ppb	92/104	[58]/2023
$In_2O_3/Ti_3C_2T_x$	5	60.6%	5 ppm	3/2	[73]/2022
$Ti_3C_2T_x/ZnO$	50	196%	1 ppm	119/307	[74]/2023
$Ti_3C_2T_x/TiO_2$	30	40.6%	5 ppm	10/5	[64]/2022
$Ti_3C_2T_x/SnO_2$	50	40%	0.5 ppm	36/44	[68]/2021
$Ti_3C_2T_x/SnO$	10	67%	1 ppm	61/119	[75]/2022
$Ti_3C_2T_x/TiO_2/CuO$	100	56.9%	10 ppm	75/80	[54]/2023
α-$Fe_2O_3/Ti_3C_2T_x$	5	18.3%	5 ppm	2.5/2	[76]/2022

3.2. Conductive Polymer Addition

Conducting polymers, such as polyaniline (PANI), polypyrrole (PPy), polydioxothiophene (PEDOT), and their derivatives, possess the advantages of high flexibility, the ability to work at room temperature, and a high response to ammonia. As a result, they are receiving increasing attention for their use in NH_3 sensing at room temperature [77,78]. To address the issues of $Ti_3C_2T_x$ MXene resistance drift, the long recovery time, the low response value, and susceptibility to mechanical deformation, it has been proposed to hybridize $Ti_3C_2T_x$ MXene with conductive polymers. This approach aims to enhance the sensitivity and wearable performance at room temperature of $Ti_3C_2T_x$ MXene through the heterojunctions formed between the two materials and the high flexibility of the conducting polymers [79,80].

Polyaniline (PANI) has been widely used in room-temperature ammonia sensors due to its strong electrical conductivity, superior selectivity to ammonia, and room-temperature workability [81,82]. Yang et al. [82] used electrostatic spinning to combine polyaniline with $Ti_3C_2T_x$ nanosheets to construct polyaniline/$Ti_3C_2T_x$ composite nanofibers with excellent ammonia responsiveness for room-temperature flexible ammonia sensors. The SEM image in Figure 5a demonstrates that the synthesized $Ti_3C_2T_x$ exhibits a distinct layer structure, and the Tyndall phenomenon can be seen in the inset. Figure 5b is an SEM image of PANI/$Ti_3C_2T_x$, which reveals a 3D network fiber structure with random fiber orientation. Figure 5c shows that the PANI/$Ti_3C_2T_x$ flexible sensor has a greater NH_3-sensing response at 25 °C (2.3 times the response value at 20 ppm compared to pure PANI), with good selectivity, repeatability, and long-term stability. Figure 5f demonstrates that by adjusting the bending angle (0°–150°) and the number of bending times (up to 3200), a high sensing performance at 20 ppm NH_3 and enduring flexible bending stability can be attained. PANI is a conductive p-type semiconductor with a band gap of about 2.47 eV [83]; the resistance of the pure $Ti_3C_2T_x$ sensor, exhibiting a metallic nature, was tested to be about 24 Ω [79], and the $Ti_3C_2T_x$ band gap was reviewed in the literature to be about 0.19 eV [68]. In the UPS results of the composites in Figure 5d,e, the figures of merit for $Ti_3C_2T_x$ and PANI/$Ti_3C_2T_x$ composite nanofibers are 2.99 eV and 3.44 eV, respectively (UV is He I, 21.22 eV). Therefore, the formation of the Schottky junction at the interface between $Ti_3C_2T_x$ and PANI enhances the resistance modulation of the flexible sensor. The gas sensitivity of the PANI/$Ti_3C_2T_x$ flexible sensor was shown to be enhanced because the composite of the PANI and $Ti_3C_2T_x$ nanosheets constitutes a Schottky junction, the degree of PANI protonation is increased, and the two are hybridized to form a special three-dimensional reticulated fibrous structure, which has great potential for the construction of flexible ammonia gas sensors.

In addition, electrostatic spinning has been widely used in conductive polymer sensors as an easy, efficient, low-cost nanofiber preparation technique. Compared with the traditional synthesis method, the electrostatic spinning method can greatly increase nanomaterials' specific surface area volume ratio [84]. By integrating polymers with nanofiber structures into resistive gas sensors, porous materials with a high surface area and large porosity can be prepared to enhance the adsorption of ammonia molecules by the sensors and improve the sensitivity of the sensors, as well as to further optimize the properties of the polymer-sensitive materials, such as their hydrophobicity, conductivity, and flexibility [85,86]. In addition, these sensors also showed fast response and recovery times. Zhang synthesized polyaniline and polymethyl methacrylate (PMMA) nanocomposite fibers using electrostatic spinning [87]. This sensitive material was shown to have a fast response and high sensitivity to NH_3, with a sensitivity of 4.5% to 5 ppm NH_3 and a response/recovery time of about 5 s/12 s. On this basis, through the composite of different conductive polymer materials and $Ti_3C_2T_x$ MXene, as well as the optimization of the electrostatic spinning process conditions, the development of NH_3-sensitive materials with a high sensing performance is expected. This is essential for further optimizing the ammonia sensor performance of the conducting polymer/$Ti_3C_2T_x$ MXene composites.

Poly (3,4-ethylenedioxythiophene):polystyrene sulfonate (PEDOT:PSS) has attracted a lot of attention in the field of gas sensing because of its good electrical conductivity, low bandgap, environmental friendliness, capacity to detect dangerous chemicals at low operating temperatures [88–91], and environmental stability [92,93]. Jin et al. [94] created PEDOT:PSS/$Ti_3C_2T_x$ MXene composites by combining 3,4-ethylenedioxythiophene (PEDOT) and poly (4-styrenesulfonate) (PSS) on a $Ti_3C_2T_x$ MXene material on a polyimide (PI) substrate through in situ polymerization. Figure 5g,h show the SEM images of $Ti_3C_2T_x$ MXene and PEDOT:PSS/$Ti_3C_2T_x$ MXene composites, respectively, where the $Ti_3C_2T_x$ exhibits a monolayered or few-layered lamellar structure after the introduction of the PEDOT:PSS, where the surface of $Ti_3C_2T_x$ MXene is covered by micro- and submicrometer PEDOT:PSS plates. Comparing Figure 5i,j reveals that the introduction of PEDOT:PSS increases the gap between the layers of the composite material. The gas sensitivity of NH_3 achieved the highest response value (Figure 5k) when $Ti_3C_2T_x$ MXene contained 15 wt% and the fastest recovery/response with 36.6% response to 100 ppm NH_3 at room temperature, a 116 s response time, and a 40 s recovery time. Furthermore, Figure 5l shows a bending test of the sensor at a maximum angle of 240°, and the gas response of the device does not change with the change in the bending angle, indicating that it has good mechanical stability.

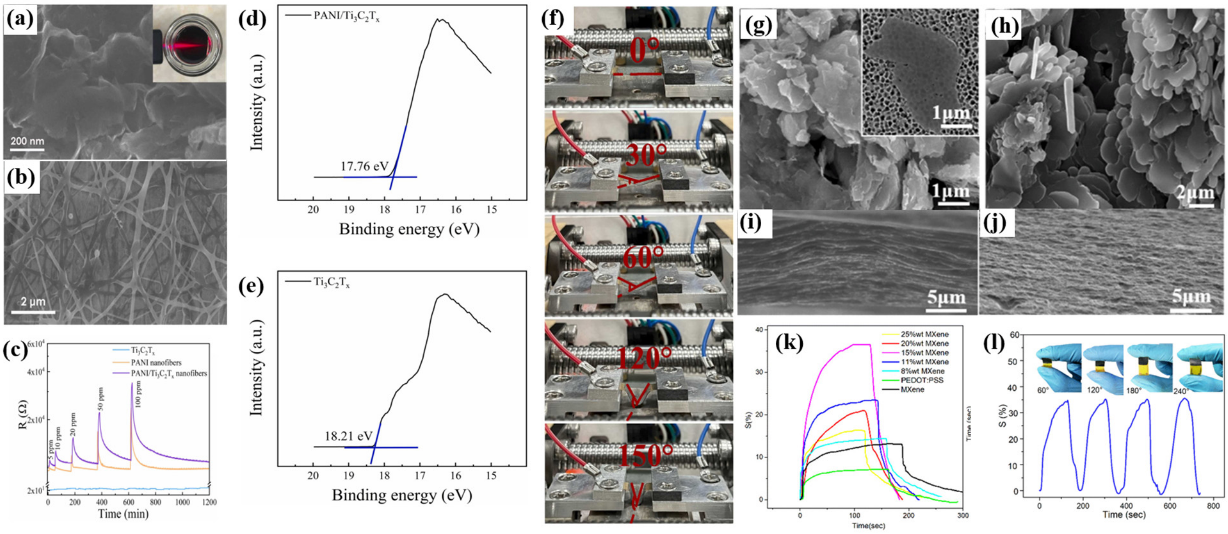

Figure 5. (**a**) SEM image of $Ti_3C_2T_x$ MXene; (**b**) SEM image of PANI/$Ti_3C_2T_x$; (**c**) PANI/$Ti_3C_2T_x$ composite nanofiber sensor for the detection of NH_3 at room temperature; (**d**) UPS spectra of pure $Ti_3C_2T_x$ sensor and (**e**) PANI/$Ti_3C_2T_x$ composite sensors; (**f**) the PANI/$Ti_3C_2T_x$-based flexible sensor bent at different angles [82]. FESEM images of (**g**) $Ti_3C_2T_x$ MXene (inset is $Ti_3C_2T_x$ MXene on an AAO membrane) and (**h**) PEDOT:PSS/$Ti_3C_2T_x$ MXene composites. The cross-sectional FESEM images of (**i**) $Ti_3C_2T_x$ MXene films and (**j**) PEDOT:PSS/$Ti_3C_2T_x$ MXene films, (**k**) effect of the $Ti_3C_2T_x$ MXene content in PEDOT-PSS on the sensor response toward 100 ppm NH_3 at room temperature (27 °C), and (**l**) gas response of the PEDOT:PSS/$Ti_3C_2T_x$ MXene composite-based sensor against 100 ppm NH_3 bent at different angles [94].

The mechanism for analyzing the gas-sensitive performance enhancement of the PEDOT:PSS/$Ti_3C_2T_x$ MXene composite mainly involves the redox reaction between the composite and the analyte, the charge transfer between the composite and the analyte, and synergistic effect of the increase in the specific surface area of the composite materials. Compared with pure PEDOT:PSS and $Ti_3C_2T_x$ MXene-based sensors, the composite sensors have a high gas response, fast response/recovery, a low detection limit, good reproducibility, high selectivity, and excellent mechanical stability. A number of studies have demonstrated that the NH_3 sensors prepared from $Ti_3C_2T_x$ MXene and conductive polymer hybrid materials have a low detection limit, flexibility, and an excellent sensing performance [95].

Table 2 outlines the gas-sensing properties of different conductive polymer /$Ti_3C_2T_x$ MXene composites towards NH_3 at room temperature that were determined in recent years.

Table 2. The gas-sensitive properties of various conductive polymer/$Ti_3C_2T_x$ MXene nanocomposites to NH_3 at room temperature.

Materials	Concentration (ppm)	Response Value (R_a/R_g, R_g/R_a) or Response Rate [($\Delta R/R_g$) × 100%]	LoD	Response/Recovery Time (s)	Ref./Year
PANI/$Ti_3C_2T_x$	10	1.6	25 ppb	—	[79]/2020
PANI:PSS/$Ti_3C_2T_x$	1	57%	20 ppb	276/388	[80]/2023
PANI/$Ti_3C_2T_x$	20	55.9%	5 ppm	—	[82]/2023
PEDOT:PSS/N-$Ti_3C_2T_x$	10	13%	10 ppm	—	[96]/2022
PANI/$Ti_3C_2T_x$/TiO_2	10	2.3	20 ppb	266/342	[24]/2023
Polyacrylamide/$Ti_3C_2T_x$	200	4.7%	—	12.7/14.6	[97]/2020
PPy/MXene	100	31.9%	5 ppm	38/383	[98]/2022
PEDOT:PSS/$Ti_3C_2T_x$	100	36.6%	10 ppm	116/40	[94]/2020
$Ti_3C_2T_x$/PDDS	0.5	2.2%	500 ppb	—	[99]/2022

3.3. Other 2D Material Hybrids

In addition to MXene, graphene, as well as various emerging 2D materials such as transition metal disulfide compounds (TMDs), reduced graphene oxide (rGO), and black phosphorus (BP), have been rapidly developed for NH_3-sensing due to their graphene-like layered structure, large specific surface area, semiconducting properties, and room-temperature operation. It has been demonstrated that the heterojunction constructed by compositing $Ti_3C_2T_x$ MXenes with these 2D materials can obtain complementary electrical and adsorption properties, which enhances their sensing performance [95].

It has been demonstrated that when MXenes are combined with TMDs, such as molybdenum disulfide (MoS_2), tin disulfide (SnS_2), tungsten disulfide (WS_2), and other transition metal disulfide compounds, their charge transfer and adsorption abilities are enhanced, which leads to better sensing effects [100,101]. In addition, the composite of TMDs and MXene has almost no lattice mismatch [102], and is expected to replace the traditional metal oxide composite with MXene to construct high-performance ammonia gas-sensitive materials [103,104]. In order to overcome the difficulty of detecting ultra-low concentrations of ammonia at room temperature in chemical-based gas sensors, He et al. [56] developed an MXene/SnS_2 heterojunction-type chemoresistive sensor SM-5 (the nominal weight ratio of MXene/SnS is 1:5), as shown in Figure 6a,b, which exhibits an excellent gas-sensitive performance for ammonia at sub-ppm at room temperature. The SM-5 sensor can detect NH_3 concentrations of as low as 10 ppb at room temperature. In addition, Figure 6c shows the excellent long-term stability of the sensor, with a decrease in response value of about 3.4% in 20 days. Meanwhile, the SM-5 sensor showed good selectivity to a wide range of possible interfering gases, such as HCHO, C_2H_5OH, CH_3OH, C_3H_6O, C_6H_6, and NO_2. The sensing mechanism of the MXene/SnS_2-based sensor is closely related to the formation of heterostructures. DFT calculations show that the higher sensitivity and selectivity may be due to the more effective charge transfer bestowed by the formed heterostructure, the better catalytical activity, and the stronger NH_3 adsorption of the formed MXene/SnS_2 composite material.

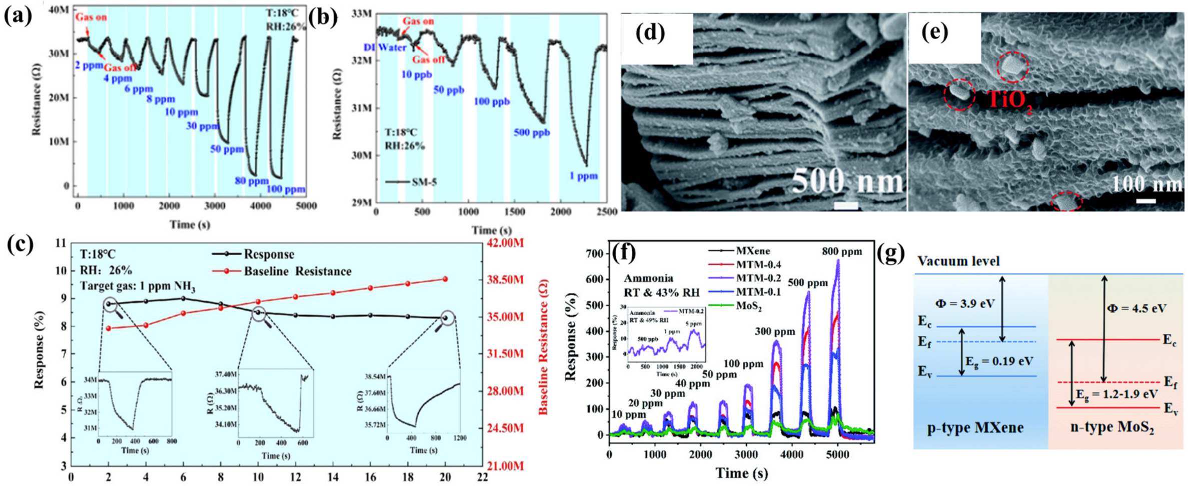

Figure 6. The resistance variation curves of the SM-5 sensor to (**a**) ppm-level NH_3 concentration from 2 to 100 ppm and (**b**) ppb-level NH_3 concentration from 10 ppb to 1 ppm at 18 °C; (**c**) the long-term stability of the SM-5 sensor to 1 ppm NH_3 for 20 days [56]. (**d**,**e**) $Ti_3C_2T_x$ MXene@TiO_2/MoS_2; (**f**) dynamic sensing performance of the sensor-based $Ti_3C_2T_x$ MXene to NH_3 at a room temperature of 27 °C and an RH of 43%; (**g**) energy band diagrams of $Ti_3C_2T_x$ MXene@TiO_2/MoS_2 sensors [30].

Our group [30] demonstrated a $Ti_3C_2T_x$ MXene@TiO_2/MoS_2 nanocomposite gas sensor, which successfully realized the detection of 500 ppb NH_3 at room temperature. MoS_2 nanosheets were grown in situ on the etched $Ti_3C_2T_x$ MXene material via the hydrothermal method, and then some of the $Ti_3C_2T_x$ MXene was converted into rectangular TiO_2 particles through hydrothermal reaction. The SEM images of $Ti_3C_2T_x$ MXene@TiO_2/MoS_2 at different scales are shown in Figure 6e; it can be observed that rectangular TiO_2 nanoparticles are attached between the layers of the material and on the surface, which increase the spacing of the layers of the composite material and can provide more reaction sites for the target gas. As shown in Figure 6f, this novel gas sensor (MTM-0.2) based on a layered structure exhibits the advantages of a fast response and high stability in detecting NH_3. At 100 ppm ammonia, the composite gas sensor had 1.79 and 2.75 times higher response values than the pristine $Ti_3C_2T_x$ MXene and MoS_2. Furthermore, at room temperature, the $Ti_3C_2T_x$ MXene@TiO_2/MoS_2 nanocomposite gas sensor exhibited high selectivity for triethylamine, trimethylamine, n-butanol, acetone, formaldehyde, and nitrogen dioxide. As shown in Figure 6g, MoS_2 is an n-type sensing material, which has a bandgap in the range of 1.2–1.9 eV [105] and a work function of about 3.9 eV [106]. $Ti_3C_2T_x$ MXene behaves as a p-type sensing material, which has a bandgap of 0.19 eV [68] and a work function of about 4.5 eV [69]. The heterojunction of the p-type $Ti_3C_2T_x$ MXene and n-type MoS_2 was the primary reason for the sensor's improved gas-sensitive performance for NH_3. Bader charge analysis can further obtain the adsorption between sensitive materials and gases by evaluating the amount of charge transfer between gas molecules and sensitive material models [107]. Bader analysis further confirmed that ammonia molecules increase charge transfer in the heterojunction, which enhances the interaction of $Ti_3C_2T_x$ MXene@TiO_2/MoS_2 nanocomposites with ammonia.

Graphene fibers (GFs) have a high mechanical flexibility, electrical conductivity, and wear ability and have enormous potential for application in wearable electronic devices [108,109]. Lee et al. [19] reported a simple, scalable, and effective strategy for wet-spinning MXene/graphene-based hybrid fibers using a wet-spinning process to obtain metal-free binder $Ti_3C_2T_x$ MXene/graphene hybrid fibers. These hybrid fibers have excellent mechanical and electrical properties, making them suitable for flexible, wearable gas sensors. The synergistic effect of the electronic properties and gas adsorption capacity of MXene/graphene resulted in a high NH_3 gas sensitivity at room temperature. Figure 7a compares the response values of MXene, rGO fiber, and MXene/rGO fiber sensors, and shows that the $Ti_3C_2T_x$ MXene/graphene hybrid fiber exhibited a significantly improved NH_3-sensing response ($\Delta R/R_0$ = 6.77%). The hybrid fiber exhibits excellent mechanical flexibility. Figure 7b depicts a schematic diagram of the device used to detect the stability of the fiber optic sensor by bending it repeatedly and detecting the change in the resistance of the sensor. As shown in Figure 7c, the resistance fluctuation remains small, ±0.2%, even after more than 2000 bends. In addition, the highly flexible MXene/rGO hybrid fiber was woven/knitted into the lab coat using a simple conventional weaving procedure, demonstrating a dependable sensing capability. The synergistic effect of the optimized bandgap and the enhanced atomic oxygen content at the MXene end of the MXene/rGO hybrid fiber significantly improved the NH_3-sensing response performance of the MXene/rGO hybrid fiber with low power consumption.

Yotsarayuth et al. [25] successfully synthesized $Ti_3C_2T_x$ Mxene/GO/CuO/ZnO nanocomposites by mixing common NH_3-sensing materials such as graphene oxide (GO), copper oxide (CuO), and zinc oxide (ZnO) into $Ti_3C_2T_x$ Mxene via a simple and low-cost hydrothermal method. Figure 7d shows the SEM images of the composites, and the $Ti_3C_2T_x$ Mxene/GO/CuO/ZnO nanocomposites exhibit a highly uniform two-dimensional stacked structure. A comparison with the SEM image of pure $Ti_3C_2T_x$ MXene in Figure 7e reveals that the composites have a high surface roughness, which enhances the active sites for the adsorption of NH_3 gas molecules. Figure 7f depicts $Ti_3C_2T_x$ MXene, GO, CuO, and ZnO figures of work functions of 4.35, 4.78, 4.7, and 5.14 eV [19,110–112], respectively, with $Ti_3C_2T_x$ MXene having the lowest figure of work function. As a result, electrons are transferred from $Ti_3C_2T_x$ MXene to the other three materials to achieve Fermi energy level equilibrium, forming multiple p-n heterojunctions at the interfaces of the different materials. $Ti_3C_2T_x$ MXene/GO/CuO/ZnO exhibits a 59.9% response to 100 ppm NH_3 at room temperature, with a response time of 26 s and a recovery time of 25 s. The $Ti_3C_2T_x$ MXene/GO/CuO/ZnO exhibits excellent selectivity, high responsiveness, good repeatability, strong stability, a quick response recovery time, and humidity independence. The $Ti_3C_2T_x$ MXene/GO/CuO/ZnO gas sensor exhibits a remarkable NH_3-sensing performance. This is because of the inherent features and properties of the nanocomposites, including their functional groups, their bonding, the strong intermolecular attraction between NH_3 molecules, the nanocomposites, and the formation of a p-n heterojunction.

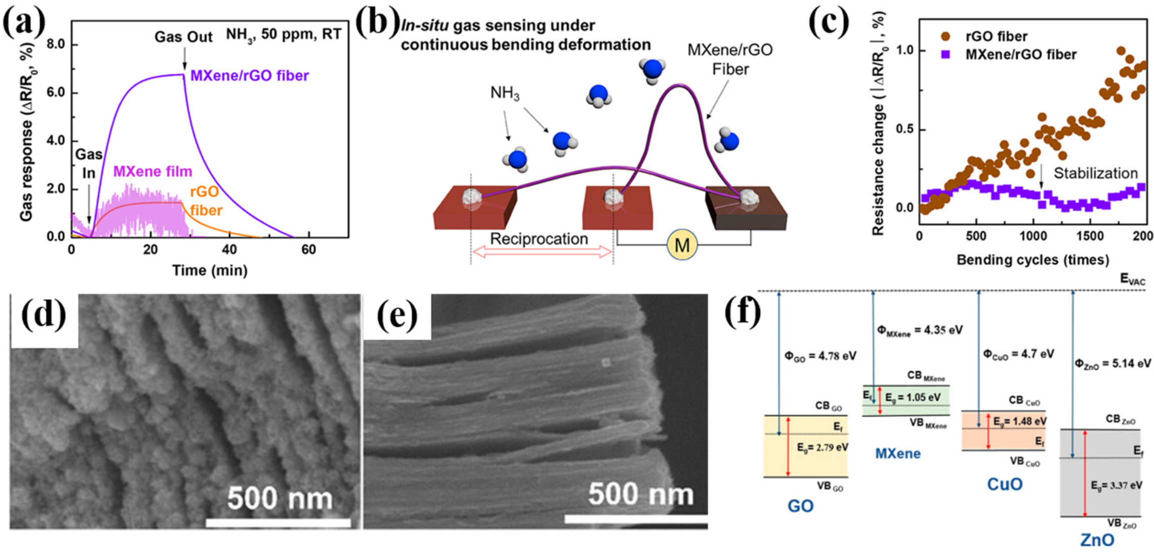

Figure 7. (**a**) Comparison of the gas response of MXene film, rGO fiber, and MXene/rGO hybrid fiber; (**b**) schematic illustration of the fiber bending test. The "M" stands for multimeter. (**c**) Cyclic bending fatigue versus resistance difference of the rGO fiber and MXene/rGO hybrid fiber [19]. (**d**) FE-SEM images of $Ti_3C_2T_x$ MXene/GO/CuO/ZnO nanocomposite and (**e**) pristine $Ti_3C_2T_x$ Mxene. (**f**) Schematic diagram of the energy band structure of the $Ti_3C_2T_x$ MXene/GO/CuO/ZnO heterostructure [25].

Table 3 outlines the gas-sensitive properties of different 2D materials/$Ti_3C_2T_x$ MXene composites towards NH_3 at room temperature.

Table 3. The gas-sensitive properties of various 2D material /$Ti_3C_2T_x$ MXene nanocomposites to NH_3 at room temperature.

Materials	Concentration (ppm)	Response Value (R_a/R_g, R_g/R_a) or Response Rate [($\Delta R/R_g$) × 100%]	LoD	Response/Recovery Time (s)	Ref./Year
$Ti_3C_2T_x$@TiO_2/MoS_2	100	163.3%	500 ppb	117/88	[30]/2022
$Ti_3C_2T_x/SnS_2$	10	42.9%	10 ppb	161/80	[56]/2023
$Ti_3C_2T_x$/rGO	50	6.77%	10 ppm	—	[19]/2020
$Ti_3C_2T_x$/GO/CuO/ZnO	100	59.9%	4.1 ppm	26/25	[25]/2023
$Ti_3C_2T_x/MoS_2$	100	81.7%	200 ppb	3/—	[110]/2022
$Ti_3C_2T_x/TiO_2$/graphene	50	36.8%	22.23 ppb	19/29	[113]/2024
$SnS/Ti_3C_2T_x$	5	1.031	250 ppb	7/—	[114]/2022

4. $Ti_3C_2T_x$ MXenes-Based Nanocomposite Material Mechanism for NH_3

The unique properties of terminating functional groups on the surface of MXenes make them ideal for ammonia-sensitive materials. Bhardwaj et al. [115] found that the effective adsorption energy of Ti_2CO_2 with NH_3 was −0.37 eV using DFT calculations, and the charge transfer between monolayer Ti_2CO_2, which has a similar structure to that of $Ti_3C_2O_2$ and NH_3, was 0.174 e. Similarly, Atkare et al. [95] discovered that MXenes, including monolayers of $Ti_3C_2O_2$, $Ti_2C(OH)_2$, and others, exhibit a significant affinity to NH_3, resulting in a charge transfer of 0.117 e.

At room temperature, the reaction mechanism of $Ti_3C_2T_x$ MXene to NH_3 molecules can consist of two parts: the reaction between NH_3 molecules and oxygen molecules on the surface of the sensitive material and the reaction between NH_3 molecules and specific functional groups at the end of $Ti_3C_2T_x$ MXene [18,57]. First, the adsorption of O_2 molecules on the surface of the sensitive material traps electrons in the form of oxygen ions, mainly in the form of O^{2-}. When the sensor is exposed to a reducing gas such as NH_3, the O^{2-} will react with the NH_3 molecules to form NO and H_2O while releasing electrons. The resistance decreases when these electrons return to the conduction band of $Ti_3C_2T_x$ MXene and its composites. The reaction process is shown in Equations (4)–(6):

$$O_2\ (\text{gas}) \rightarrow O_2\ (\text{ads}) \tag{4}$$

$$O_2(\text{ads}) + e^- \rightarrow O_2^- \tag{5}$$

$$4NH_3 + O_2^- \rightarrow 4NO + 6H_2O + 5e^- \tag{6}$$

The gas-sensing mechanism of $Ti_3C_2T_x/In_2O_3$ composites to NH_3 shown in Figure 8b can be used as a reference. In addition to the electron transfer process between oxygen ions and NH_3 molecules on the surface of $Ti_3C_2T_x$ MXene-sensitive materials, Lee et al. [57] mentioned that the reaction of -O and -OH on the surface of $Ti_3C_2T_x$ with NH_3 resulted in hole–electron complexation and a subsequent increase in resistance, and the conjectured mechanism diagram is shown in Figure 8a. The reaction formulae are shown in Equations (7) and (8) as follows:

$$2NH_3 + 3O^- \rightarrow N_2 + 3H_2O + 3e^- \tag{7}$$

$$NH_3 + OH^- \rightarrow NH_2 + H_2O + e^- \tag{8}$$

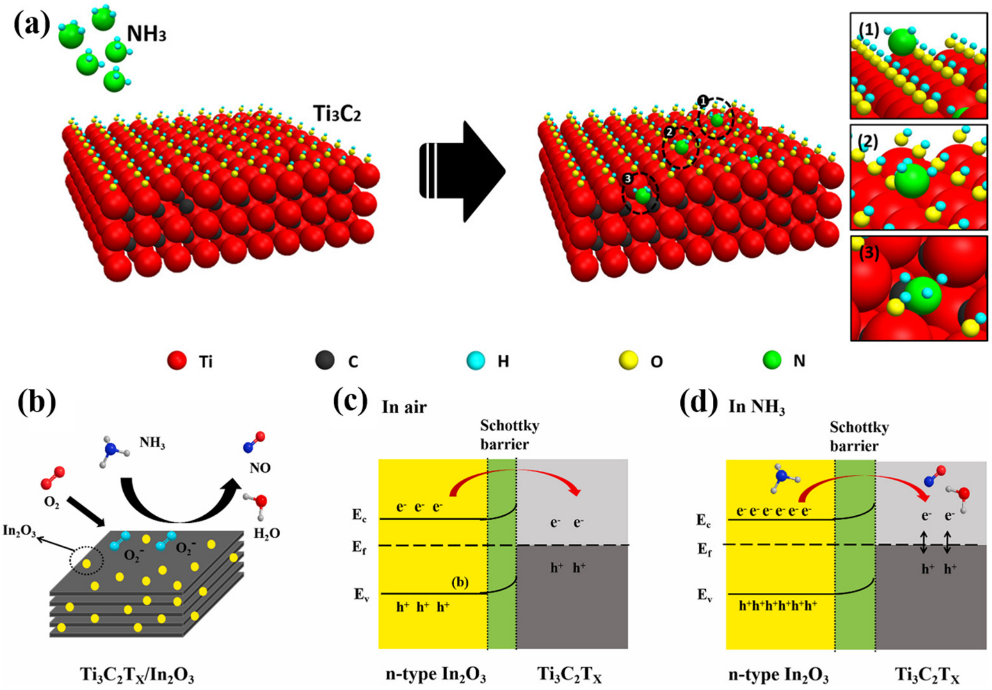

Figure 8. (**a**) Schematic diagram of the possible gas-sensing mechanisms of the $Ti_3C_2T_x$ MXene for NH_3 [18]. (**b**) The gas-sensing mechanism diagram of the $Ti_3C_2T_x/In_2O_3$ composite materials. (**c**,**d**) Schematic diagram of the electron transfer at the interface of $Ti_3C_2T_x/In_2O_3$ composite materials in the air and NH_3 [57].

The mechanism for the enhanced gas sensitivity of $Ti_3C_2T_x$ MXene composite materials to NH_3 is generally achieved by the synergistic effect between the two materials, such as the formation of a heterojunction of the composites, adsorption energy and charge transfer, chemical sensitization and electron sensitization, unique morphology, etc. [11,61]. When heterojunctions are formed, the gap in the work function between $Ti_3C_2T_x$ MXene and its composite material causes electrons to transfer directionally from the lower to the higher work function. This transfer occurs due to the equilibrium of the Fermi energy levels when the materials come into contact with each other. This results in the formation of an electron depletion layer and an electron accumulation layer on the low-work-function material. The electron accumulation layer promotes oxygen adsorption on the surface of the sensing material. In contrast, the electron depletion layer increases the potential energy barrier at the interface, while the height of the intergranular barrier hinders the transport of carriers, resulting in an increase in the initial resistance [116] and a higher gas response. As an illustration, Zhou et al. [57] synthesized $Ti_3C_2T_x/In_2O_3$ nanocomposites. In_2O_3 is classified as an n-type semiconductor, while $Ti_3C_2T_x$ is regarded as a metallic phase because of its excellent conductivity. When $Ti_3C_2T_x$ comes into contact with In_2O_3, it exhibits a high work function. As a result, electrons migrate from In_2O_3 to $Ti_3C_2T_x$, forming a Schottky barrier and a depletion layer at the interface of In_2O_3 and $Ti_3C_2T_x$ (as shown in Figure 8c,d). As a result, the charge transfer is blocked, and the base-value resistance of $Ti_3C_2T_x/In_2O_3$ becomes high in the air, resulting in a significant increase in the gas-sensitive response [22]. In addition, the improved gas-sensitive performance of the sensitive material is also related to its lattice mismatch, and the oxygen vacancies generated at the heterojunction due to the lattice mismatch will also provide additional active sites for the sensitive material [117].

The most significant characteristic of MXenes is their demonstration of similar metallic properties to their precursor MAX, with a fixed electron density near the Fermi energy level. In fact, the gas-sensing mechanism of MXene is notably more complex than the classical charge transfer model [95]. Lee et al. [18] were the first to report the gas-sensing mechanism of $Ti_3C_2T_x$ MXene. They observed increased resistance in $Ti_3C_2T_x$ sensors when exposed to four electron donor gases (ethanol, methanol, acetone, and ammonia). Conversely, the resistance of $Ti_3C_2T_x$ films decreased without the presence of these gases. Therefore, they inferred that $Ti_3C_2T_x$ films exhibit p-type sensing behavior. The analysis suggests that the p-type semiconductor nature of $Ti_3C_2T_x$ MXene may be due to the many molecules introduced during the Al etching process acting as p-type dopants to $Ti_3C_2T_x$, such as water and oxygen.

It is well known that gas sensors for semiconductor materials exhibit either a positive or negative resistance change depending on the gas type [118]. Specifically, an n-type semiconductor-sensitive material exposed to oxidizing gases decreases in resistance due to the loss of electrons and increases due to the gain in electrons when exposed to reducing gases, and the opposite is true for p-type semiconductor-sensitive materials. In contrast, Kim et al. [118] found that $Ti_3C_2T_x$ exhibits a positive resistance change under oxidized or reduced gas conditions, indicating that the carrier transport of $Ti_3C_2T_x$ will be blocked when it adsorbs gases. In other words, the sensing mechanism of $Ti_3C_2T_x$ is different from that of semiconductor materials such as metal oxides. Therefore, the mechanism for the universal p-type response of $Ti_3C_2T_x$ was proposed. Due to the metallic conductivity of $Ti_3C_2T_x$ MXene [119], the gas adsorption reduces the number of carriers and therefore increases the channel resistance. While Koh et al. [120] investigated the effect of the interlayer swelling of $Ti_3C_2T_x$ MXene films upon gas action on the gas-sensitive properties, the change in the interlayer space of $Ti_3C_2T_x$ MXene upon the introduction of gas was studied by in situ XRD measurements, which found that the degree of swelling of $Ti_3C_2T_x$ MXene films was consistent with the gas response. Therefore, another mechanism is proposed: gas-phase molecules are inserted into the MXene interlayer instead of surface adsorption, and the interlayer expansion induced to reduce the conductivity due to the metallic nature of $Ti_3C_2T_x$ MXene is one of the reasons why MXene generally exhibits a p-type response to various gases.

Both mechanisms currently explain MXene's p-type response to the electron acceptor gas and the electron donor gas. To date, the gas-sensing mechanism of $Ti_3C_2T_x$ MXene and its composites has not been explained in a unified manner. The electron transfer model of the adsorbed gas molecules on the surface of $Ti_3C_2T_x$ composites may be more complex than reported and thus needs to be further developed and refined through experimental validation.

5. Conclusions and Outlook

$Ti_3C_2T_x$ MXene, as the earliest discovered MXene material, which has been extensively studied in the field of ammonia gas sensing, has been regarded as an excellent room-temperature NH_3-sensing material due to its graphene-like two-dimensional lamellar structure, which confers a large specific surface area, good room-temperature sensitivity, and a high adsorption capacity between its surface-rich functional groups and NH_3. This review describes the current research progress in modulating the ammonia gas-sensing properties of $Ti_3C_2T_x$ MXene by means of its preparation method and composite modification. $Ti_3C_2T_x$ MXene with differences in its morphology, surface functional groups, electrochemical properties, nano-defects, and stability can be obtained through improvements in the preparation method to achieve the desired performance, which in turn affects the NH_3-sensing behavior of the sensors. $Ti_3C_2T_x$ MXene-based composites incorporating additional composites can demonstrate enhanced response values, lower detection limits, quicker response recovery, and an improved stability compared to pure $Ti_3C_2T_x$ MXene.

Although significant progress has been made in the design and modification of $Ti_3C_2T_x$ MXene materials for ammonia gas sensors in recent years, there are still many challenges and much room for further development in optimizing and improving the sensing performance. Since the gas-sensing mechanism of MXenes is much more complex than the traditional semiconductor classical charge-transfer model, further calculations and investigations regarding the charge transfer and adsorption–desorption are needed in terms of the NH_3-sensing principle of $Ti_3C_2T_x$ MXene. Meanwhile, a large number of studies have demonstrated that the surface-functional groups of $Ti_3C_2T_x$ MXene have a significant effect on its electrochemical properties and stability. Therefore, synthesizing $Ti_3C_2T_x$ MXene materials with controllable surface-functional groups is significant for its application in room-temperature ammonia gas sensors. Furthermore, $Ti_3C_2T_x$ MXene's composite structure can be further optimized to improve its NH_3-sensing performance. In the next step, we could design $Ti_3C_2T_x$ MXene sensors with excellent long-term stability and a response value that is less impacted by humidity to widen their applications. In the future, we should broaden our research on $Ti_3C_2T_x$ MXene in these fields to develop higher-performance $Ti_3C_2T_x$ MXene-based room-temperature ammonia sensors.

Funding: This research received no external funding.

Acknowledgments: The authors would like to show their gratitude to Yunnan Key Laboratory of Carbon Neutrality and Green Low-Carbon Technologies (No. 202205AG070002 (Y.W.)), the National Natural Science Foundation of China (No. 41876055 and 61761047 (Y.W.)).

Conflicts of Interest: The authors declare no conflict of interest.

References

1. Garg, N.; Kumar, M.; Kumari, N.; Deep, A.; Sharma, A.L. Chemoresistive room-temperature sensing of ammonia using zeolite imidazole framework and reduced graphene oxide (ZIF-67/rGO) composite. *ACS Omega* **2020**, *5*, 27492–27501. [CrossRef] [PubMed]
2. Yap, S.H.K.; Chan, K.K.; Tjin, S.C.; Yong, K.T. Carbon allotrope-based optical fibers for environmental and biological sensing: A review. *Sensors* **2020**, *20*, 2046. [CrossRef] [PubMed]
3. Zhu, C.; Zhou, T.; Xia, H.; Zhang, T. Flexible room-temperature ammonia gas sensors based on PANI-MWCNTs/PDMS film for breathing analysis and food safety. *Nanomaterials* **2023**, *13*, 1158. [CrossRef] [PubMed]
4. Fairose, S.; Ernest, S.; Daniel, S. Effect of oxygen sputter pressure on the structural, morphological and optical properties of ZnO thin films for gas sensing application. *Sens. Imaging* **2018**, *19*, 1. [CrossRef]

5. Seekaew, Y.; Pon-On, W.; Wongchoosuk, C. Ultrahigh selective room-temperature ammonia gas sensor based on tin-titanium dioxide/reduced graphene/carbon nanotube nanocomposites by the solvothermal method. *ACS Omega* **2019**, *4*, 16916–16924. [CrossRef] [PubMed]
6. Gao, R.; Ma, X.; Liu, L.; Gao, S.; Zhang, X.; Xu, Y.; Cheng, X.; Zhao, H.; Huo, L. In-situ deposition of POMA/ZnO nanorods array film by vapor phase polymerization for detection of trace ammonia in human exhaled breath at room temperature. *Anal. Chim. Acta* **2022**, *1199*, 339563. [CrossRef] [PubMed]
7. Wei, H.; Zhang, H.; Song, B.; Yuan, K.; Xiao, H.; Cao, Y.; Cao, Q. Metal-organic framework (MOF) derivatives as promising chemiresistive gas sensing materials: A review. *Int. J. Environ. Res. Public Health* **2023**, *20*, 4388. [CrossRef] [PubMed]
8. Zhang, S.; Jia, Z.; Liu, T.; Wei, G.; Su, Z. Electrospinning nanoparticles-based materials interfaces for sensor applications. *Sensors* **2019**, *19*, 3977. [CrossRef] [PubMed]
9. Wang, X.-F.; Song, X.-Z.; Sun, K.-M.; Cheng, L.; Ma, W. MOFs-derived porous nanomaterials for gas sensing. *Polyhedron* **2018**, *152*, 155–163. [CrossRef]
10. Tai, H.; Yuan, Z.; Zheng, W.; Ye, Z.; Liu, C.; Du, X. ZnO nanoparticles/reduced graphene oxide bilayer thin films for improved NH_3-sensing performances at room temperature. *Nanoscale Res. Lett.* **2016**, *11*, 130. [CrossRef]
11. Maity, A.; Raychaudhuri, A.K.; Ghosh, B. High sensitivity NH_3 gas sensor with electrical readout made on paper with perovskite halide as sensor material. *Sci. Rep.* **2019**, *9*, 7777. [CrossRef]
12. Tian, X.; Wang, S.; Yao, B.; Wang, Z.; Chen, T.; Xiao, X.; Wang, Y. Edge sulfur vacancies riched MoS_2 nanosheets assist PEDOT:PSS flexible film ammonia sensing enhancement for wireless greenhouse vegetables monitoring. *J. Hazard. Mater.* **2024**, *465*, 133195. [CrossRef]
13. Jimmy, J.; Kandasubramanian, B. Mxene functionalized polymer composites: Synthesis and applications. *Eur. Polym. J.* **2020**, *122*, 109367. [CrossRef]
14. Naguib, M.; Kurtoglu, M.; Presser, V.; Lu, J.; Niu, J.; Heon, M.; Hultman, L.; Gogotsi, Y.; Barsoum, M.W. Two-dimensional nanocrystals produced by exfoliation of Ti_3AlC_2. *Adv. Mater.* **2011**, *23*, 4248–4253. [CrossRef]
15. Qin, R.; Shan, G.; Hu, M.; Huang, W. Two-dimensional transition metal carbides and/or nitrides (MXenes) and their applications in sensors. *Mater. Today Phys.* **2021**, *21*, 100527. [CrossRef]
16. Zhang, H.-F.; Xuan, J.-Y.; Zhang, Q.; Sun, M.-L.; Jia, F.-C.; Wang, X.-M.; Yin, G.-C.; Lu, S.-Y. Strategies and challenges for enhancing performance of MXene-based gas sensors: A review. *Rare Met.* **2022**, *41*, 3976–3999. [CrossRef]
17. Xiong, D.; Shi, Y.; Yang, H.Y. Rational design of MXene-based films for energy storage: Progress, prospects. *Mater. Today* **2021**, *46*, 183–211. [CrossRef]
18. Lee, E.; VahidMohammadi, A.; Prorok, B.C.; Yoon, Y.S.; Beidaghi, M.; Kim, D.-J. Room temperature gas sensing of two-dimensional titanium carbide (MXene). *ACS Appl. Mater. Interfaces* **2017**, *9*, 37184–37190. [CrossRef]
19. Lee, S.H.; Eom, W.; Shin, H.; Ambade, R.B.; Bang, J.H.; Kim, H.W.; Han, T.H. Room-temperature, highly durable $Ti_3C_2T_x$ MXene/graphene hybrid fibers for NH_3 gas sensing. *ACS Appl. Mater. Interfaces* **2020**, *12*, 10434–10442. [CrossRef]
20. Mirzaei, A.; Lee, M.H.; Safaeian, H.; Kim, T.U.; Kim, J.Y.; Kim, H.W.; Kim, S.S. Room temperature chemiresistive gas sensors based on 2D MXenes. *Sensors* **2023**, *23*, 8829. [CrossRef]
21. Simonenko, E.P.; Simonenko, N.P.; Mokrushin, A.S.; Simonenko, T.L.; Gorobtsov, P.Y.; Nagornov, I.A.; Korotcenkov, G.; Sysoev, V.V.; Kuznetsov, N.T. Application of titanium carbide MXenes in chemiresistive gas sensors. *Nanomaterials* **2023**, *13*, 850. [CrossRef] [PubMed]
22. Tai, H.; Duan, Z.; He, Z.; Li, X.; Xu, J.; Liu, B.; Jiang, Y. Enhanced ammonia response of $Ti_3C_2T_x$ nanosheets supported by TiO_2 nanoparticles at room temperature. *Sens. Actuators B Chem.* **2019**, *298*, 126874. [CrossRef]
23. Qin, Y.; Gui, H.; Bai, Y.; Liu, S. Enhanced NH_3 sensing performance at ppb level derived from $Ti_3C_2T_x$-supported ZnTi-LDHs nanocomposite with similar metal-semiconductor heterostructure. *Sens. Actuators B Chem.* **2022**, *352*, 131077. [CrossRef]
24. Xiong, J.; Cai, Y.; Nie, X.; Wang, Y.; Song, H.; Sharif, H.M.A.; Li, Z.; Li, C. PANI/3D crumpled $Ti_3C_2T_x/TiO_2$ nanocomposites for flexible conductometric NH_3 sensors working at room temperature. *Sens. Actuators B Chem.* **2023**, *390*, 133987. [CrossRef]
25. Seekaew, Y.; Kamlue, S.; Wongchoosuk, C. Room-temperature ammonia gas sensor based on $Ti_3C_2T_x$ MXene/graphene oxide/CuO/ZnO nanocomposite. *ACS Appl. Nano Mater.* **2023**, *6*, 9008–9020. [CrossRef]
26. Mirabella, D.A.; Buono, C.; Aldao, C.M.; Resasco, D.E. Chemisorption and sensitivity at semiconductor sensors revisited. *Sens. Actuators B Chem.* **2019**, *285*, 232–239. [CrossRef]
27. Haick, H.; Ambrico, M.; Ligonzo, T.; Tung, R.T.; Cahen, D. Controlling semiconductor/metal junction barriers by incomplete, nonideal molecular monolayers. *J. Am. Chem. Soc.* **2006**, *128*, 6854–6869. [CrossRef]
28. Turaeva, N.; Krueger, H. Wolkenstein's model of size effects in CO oxidation by gold nanoparticles. *Catalysts* **2020**, *10*, 288. [CrossRef]
29. Ng, W.H.K.; Gnanakumar, E.S.; Batyrev, E.; Sharma, S.K.; Pujari, P.K.; Greer, H.F.; Zhou, W.; Sakidja, R.; Rothenberg, G.; Barsoum, M.W.; et al. The Ti_3AlC_2 MAX phase as an efficient catalyst for oxidative dehydrogenation of n-Butane. *Angew. Chem. Int. Ed.* **2018**, *57*, 1485–1490. [CrossRef]
30. Tian, X.; Yao, L.; Cui, X.; Zhao, R.; Chen, T.; Xiao, X.; Wang, Y. A two-dimensional $Ti_3C_2T_x$ MXene@TiO_2/MoS_2 heterostructure with excellent selectivity for the room temperature detection of ammonia. *J. Mater. Chem. A* **2022**, *10*, 5505–5519. [CrossRef]
31. Naguib, M.; Mochalin, V.N.; Barsoum, M.W.; Gogotsi, Y. 25th anniversary article: MXenes: A new family of two-dimensional materials. *Adv. Mater.* **2014**, *26*, 992–1005. [CrossRef] [PubMed]

32. Mashtalir, O.; Naguib, M.; Dyatkin, B.; Gogotsi, Y.; Barsoum, M.W. Kinetics of aluminum extraction from Ti_3AlC_2 in hydrofluoric acid. *Mater. Chem. Phys.* **2013**, *139*, 147–152. [CrossRef]
33. Lian, W.; Mai, Y.; Liu, C.; Zhang, L.; Li, S.; Jie, X. Two-dimensional Ti_3C_2 coating as an emerging protective solid-lubricant for tribology. *Ceram. Int.* **2018**, *44*, 20154–20162. [CrossRef]
34. Xuan, J.; Wang, Z.; Chen, Y.; Liang, D.; Cheng, L.; Yang, X.; Liu, Z.; Ma, R.; Sasaki, T.; Geng, F. Organic-Base-Driven intercalation and delamination for the production of functionalized titanium carbide nanosheets with superior photothermal therapeutic performance. *Angew. Chem. Int. Ed.* **2016**, *55*, 14569–14574. [CrossRef] [PubMed]
35. Dillon, A.D.; Ghidiu, M.J.; Krick, A.L.; Griggs, J.; May, S.J.; Gogotsi, Y.; Barsoum, M.W.; Fafarman, A.T. Highly conductive optical quality solution-processed films of 2D titanium carbide. *Adv. Funct. Mater.* **2016**, *26*, 4162–4168. [CrossRef]
36. Song, M.; Pang, S.-Y.; Guo, F.; Wong, M.-C.; Hao, J. Fluoride-free 2D niobium carbide MXenes as stable and biocompatible nanoplatforms for electrochemical biosensors with ultrahigh sensitivity. *Adv. Sci.* **2020**, *7*, 2001546. [CrossRef]
37. Ghidiu, M.; Lukatskaya, M.R.; Zhao, M.-Q.; Gogotsi, Y.; Barsoum, M.W. Conductive two-dimensional titanium carbide 'clay' with high volumetric capacitance. *Nature* **2014**, *516*, 78–81. [CrossRef] [PubMed]
38. Mashtalir, O.; Naguib, M.; Mochalin, V.N.; Dall'Agnese, Y.; Heon, M.; Barsoum, M.W.; Gogotsi, Y. Intercalation and delamination of layered carbides and carbonitrides. *Nat. Commun.* **2013**, *4*, 1716. [CrossRef]
39. Han, D.; Liu, Z.-H.; Liu, L.-L.; Han, X.-M.; Liu, D.-M.; Zhuo, K.; Sang, S.-B. Preparation and gas sensing properties of a novel two-dimensional material $Ti_3C_2T_x$ MXene. *Acta Phys. Sin.* **2022**, *71*, 010701-1–010701-9. [CrossRef]
40. Yang, Z.; Liu, A.; Wang, C.; Liu, F.; He, J.; Li, S.; Wang, J.; You, R.; Yan, X.; Sun, P.; et al. Improvement of gas and humidity sensing properties of organ-like MXene by alkaline treatment. *ACS Sens.* **2019**, *4*, 1261–1269. [CrossRef]
41. Tian, Z.; Tian, H.; Cao, K.; Bai, S.; Peng, Q.; Wang, Y.; Zhu, Q. Facile preparation of $Ti_3C_2T_x$ sheets by selectively etching in a H_2SO_4/H_2O_2 mixture. *Front. Chem.* **2022**, *10*, 962528. [CrossRef] [PubMed]
42. Wang, P.; Wang, B.; Wang, R. Progress in the synthesis process and electrocatalytic application of MXene materials. *Materials* **2023**, *16*, 6816. [CrossRef] [PubMed]
43. Yang, J.; Bao, W.; Jaumaux, P.; Zhang, S.; Wang, C.; Wang, G. MXene-Based composites: Synthesis and applications in rechargeable batteries and supercapacitors. *Adv. Mater. Interfaces* **2019**, *6*, 1802004. [CrossRef]
44. Nan, J.; Guo, X.; Xiao, J.; Li, X.; Chen, W.; Wu, W.; Liu, H.; Wang, Y.; Wu, M.; Wang, G. Nanoengineering of 2D MXene-based materials for energy storage applications. *Small* **2021**, *17*, 1902085. [CrossRef] [PubMed]
45. Qian, A.; Wu, H.; Wang, G.; Sun, N.; Cheng, H.; Zhang, K.; Cheng, F. Freeing fluoride termination of $Ti_3C_2T_x$ via electrochemical etching for high-performance capacitive deionization. *ACS Appl. Mater. Interfaces* **2023**, *15*, 9203–9211. [CrossRef] [PubMed]
46. Fan, Z.; Wang, Y.; Xie, Z.; Wang, D.; Yuan, Y.; Kang, H.; Su, B.; Cheng, Z.; Liu, Y. Modified MXene/holey graphene films for advanced supercapacitor electrodes with superior energy storage. *Adv. Sci.* **2018**, *5*, 1800750. [CrossRef] [PubMed]
47. Hu, M.; Li, Z.; Hu, T.; Zhu, S.; Zhang, C.; Wang, X. High-Capacitance mechanism for $Ti_3C_2T_x$ MXene by in situ electrochemical raman spectroscopy investigation. *ACS Nano* **2016**, *10*, 11344–11350. [CrossRef] [PubMed]
48. Ding, Y.; Zhang, J.; Guan, A.; Wang, Q.; Li, S.; Al-Enizi, A.M.; Qian, L.; Zhang, L.; Zheng, G. Promoting N_2 electroreduction to ammonia by fluorine-terminating $Ti_3C_2T_x$ MXene. *Nano Converg.* **2021**, *8*, 14. [CrossRef] [PubMed]
49. Ghazaly, A.E.; Ahmed, H.; Rezk, A.R.; Halim, J.; Persson, P.O.Å.; Yeo, L.Y.; Rosen, J. Ultrafast, one-step, salt-solution-based acoustic synthesis of Ti_3C_2 MXene. *ACS Nano* **2021**, *15*, 4287–4293. [CrossRef]
50. Lipatov, A.; Alhabeb, M.; Lukatskaya, M.R.; Boson, A.; Gogotsi, Y.; Sinitskii, A. Effect of synthesis on quality, electronic properties and environmental stability of individual monolayer Ti_3C_2 MXene flakes. *Adv. Electron. Mater.* **2016**, *2*, 1600255. [CrossRef]
51. Halim, J.; Lukatskaya, M.R.; Cook, K.M.; Lu, J.; Smith, C.R.; Näslund, L.-Å.; May, S.J.; Hultman, L.; Gogotsi, Y.; Eklund, P.; et al. Transparent conductive two-dimensional titanium carbide epitaxial thin films. *Chem. Mater.* **2014**, *26*, 2374–2381. [CrossRef] [PubMed]
52. Wu, X.; Gong, Y.; Yang, B.; Mao, Z.; Yan, Z.; Su, C.; Xiong, S.; Long, X.; Wang, X. Fabrication of SnO_2-TiO_2-$Ti_3C_2T_x$ hybrids with multiple-type heterojunctions for enhanced gas sensing performance at room temperature. *Appl. Surf. Sci.* **2022**, *581*, 152364. [CrossRef]
53. Sai Bhargava Reddy, M.; Aich, S. Recent progress in surface and heterointerface engineering of 2D MXenes for gas sensing applications. *Coord. Chem. Rev.* **2024**, *500*, 215542. [CrossRef]
54. Hou, M.; Jiang, G.; Guo, S.; Gao, J.; Shen, Z.; Wang, Z.; Ye, X.; Yang, L.; Du, Q.; Yi, J.; et al. Mxene $Ti_3C_2T_x$ derived lamellar $Ti_3C_2T_x$-TiO_2-CuO heterojunction: Significantly improved ammonia sensor performance. *Arab. J. Chem.* **2023**, *16*, 104808. [CrossRef]
55. Wu, M.; He, M.; Hu, Q.; Wu, Q.; Sun, G.; Xie, L.; Zhang, Z.; Zhu, Z.; Zhou, A. Ti_3C_2 MXene-based sensors with high selectivity for NH_3 detection at room temperature. *ACS Sens.* **2019**, *4*, 2763–2770. [CrossRef] [PubMed]
56. He, T.; Sun, S.; Huang, B.; Li, X. MXene/SnS_2 heterojunction for detecting sub-ppm NH_3 at room temperature. *ACS Appl. Mater. Interfaces* **2023**, *15*, 4194–4207. [CrossRef]
57. Zhou, M.; Han, Y.; Yao, Y.; Xie, L.; Zhao, X.; Wang, J.; Zhu, Z. Fabrication of $Ti_3C_2T_x/In_2O_3$ nanocomposites for enhanced ammonia sensing at room temperature. *Ceram. Int.* **2022**, *48*, 6600–6607. [CrossRef]
58. Pasupuleti, K.S.; Thomas, A.M.; Vidyasagar, D.; Rao, V.N.; Yoon, S.-G.; Kim, Y.-H.; Kim, S.-G.; Kim, M.-D. ZnO@$Ti_3C_2T_x$ MXene hybrid composite-based schottky-barrier-coated SAW sensor for effective detection of sub-ppb-level NH_3 at room temperature under UV illumination. *ACS Mater. Lett.* **2023**, *5*, 2739–2746. [CrossRef]

59. Tang, W.; Wang, J. Enhanced gas sensing mechanisms of metal oxide heterojunction gas sensors. *Acta Phys. Chim. Sin.* **2016**, *32*, 1087–1104. [CrossRef]
60. Pasupuleti, K.S.; Chougule, S.S.; Vidyasagar, D.; Bak, N.-h.; Jung, N.; Kim, Y.-H.; Lee, J.-H.; Kim, S.-G.; Kim, M.-D. UV light driven high-performance room temperature surface acoustic wave NH_3 gas sensor using sulfur-doped g-C_3N_4 quantum dots. *Nano Res.* **2023**, *16*, 7682–7695. [CrossRef]
61. Zhao, Q.-N.; Zhang, Y.-J.; Duan, Z.-H.; Wang, S.; Liu, C.; Jiang, Y.-D.; Tai, H.-L. A review on $Ti_3C_2T_x$-based nanomaterials: Synthesis and applications in gas and humidity sensors. *Rare Met.* **2021**, *40*, 1459–1476. [CrossRef]
62. Xiong, S.; Zhou, J.; Wu, J.; Li, H.; Zhao, W.; He, C.; Liu, Y.; Chen, Y.; Fu, Y.; Duan, H. High performance acoustic wave nitrogen dioxide sensor with ultraviolet activated 3D porous architecture of Ag-decorated reduced graphene oxide and polypyrrole aerogel. *ACS Appl. Mater. Interfaces* **2021**, *13*, 42094–42103. [CrossRef] [PubMed]
63. Sun, X.; Chen, T.; Liang, Y.; Zhang, C.; Zhai, S.; Sun, J.; Wang, W. Enhanced sensitivity of SAW based ammonia sensor employing GO-SnO_2 nanocomposites. *Sens. Actuators B Chem.* **2023**, *375*, 132884. [CrossRef]
64. Zhang, D.; Yu, S.; Wang, X.; Huang, J.; Pan, W.; Zhang, J.; Meteku, B.E.; Zeng, J. UV illumination-enhanced ultrasensitive ammonia gas sensor based on (001)TiO_2/MXene heterostructure for food spoilage detection. *J. Hazard. Mater.* **2022**, *423*, 127160. [CrossRef] [PubMed]
65. Kan, Z.; Shi, F.; Yang, L.; Zhou, Q.; Zhang, Y.; Qi, Y.; Zhang, H.; Dong, B.; Ren, L.; Song, H.; et al. A dual-mode foam sensor employing $Ti_3C_2T_x$/In_2O_3 composites for NH_3 detection with memory function and body movement monitoring for kidney disease diagnosis. *J. Mater. Chem. A* **2023**, *11*, 24299–24310. [CrossRef]
66. Liu, J.; Lin, X.; Sun, M.; Du, B.; Li, L.; Bai, J.; Zhou, M. Thiourea-assistant growth of In_2O_3 porous pompon assembled from 2D nanosheets for enhanced ethanol sensing performance. *Talanta* **2020**, *219*, 121323. [CrossRef] [PubMed]
67. Zhang, D.; Yang, Z.; Li, P.; Zhou, X. Ozone gas sensing properties of metal-organic frameworks-derived In_2O_3 hollow microtubes decorated with ZnO nanoparticles. *Sens. Actuators B Chem.* **2019**, *301*, 127081. [CrossRef]
68. He, T.; Liu, W.; Lv, T.; Ma, M.; Liu, Z.; Vasiliev, A.; Li, X. MXene/SnO_2 heterojunction based chemical gas sensors. *Sens. Actuators B Chem.* **2021**, *329*, 129275. [CrossRef]
69. Britnell, L.; Ribeiro, R.M.; Eckmann, A.; Jalil, R.; Belle, B.D.; Mishchenko, A.; Kim, Y.J.; Gorbachev, R.V.; Georgiou, T.; Morozov, S.V.; et al. Strong light-matter interactions in heterostructures of atomically Thin films. *Science* **2013**, *340*, 1311–1314. [CrossRef]
70. Guo, X.; Ding, Y.; Kuang, D.; Wu, Z.; Sun, X.; Du, B.; Liang, C.; Wu, Y.; Qu, W.; Xiong, L.; et al. Enhanced ammonia sensing performance based on MXene-$Ti_3C_2T_x$ multilayer nanoflakes functionalized by tungsten trioxide nanoparticles. *J. Colloid Interface Sci.* **2021**, *595*, 6–14. [CrossRef]
71. Yang, J.; Gui, Y.; Wang, Y.; He, S. NiO/$Ti_3C_2T_x$ MXene nanocomposites sensor for ammonia gas detection at room temperature. *J. Ind. Eng. Chem.* **2023**, *119*, 476–484. [CrossRef]
72. Liu, M.; Ding, Y.; Lu, Z.; Song, P.; Wang, Q. Layered $Ti_3C_2T_x$ MXene/CuO spindles composites for NH_3 detection at room-temperature. *J. Alloys Compd.* **2023**, *938*, 168563. [CrossRef]
73. Liu, M.; Wang, J.; Song, P.; Ji, J.; Wang, Q. Metal-organic frameworks-derived In_2O_3 microtubes/$Ti_3C_2T_x$ MXene composites for NH_3 detection at room temperature. *Sens. Actuators B Chem.* **2022**, *361*, 131755. [CrossRef]
74. Yao, L.J.; Tian, X.; Cui, X.X.; Zhao, R.J.; Chen, T.; Xiao, X.C.; Wang, Y.D. Low operating temperature and highly selective NH_3 chemiresistive gas sensors based on a novel 2D $Ti_3C_2T_x$/ZnO composite with p–n heterojunction. *Appl. Phys. Rev.* **2023**, *10*, 031414. [CrossRef]
75. Yao, L.; Tian, X.; Cui, X.; Zhao, R.; Xiao, M.; Wang, B.; Xiao, X.; Wang, Y. Two-dimensional $Ti_3C_2T_x$ MXene/SnO nanocomposites: Towards enhanced response and selective ammonia vapor sensor at room temperature. *Sens. Actuators B Chem.* **2022**, *358*, 131501. [CrossRef]
76. Liu, M.; Ji, J.; Song, P.; Wang, J.; Wang, Q. Sensing performance of α-Fe_2O_3/$Ti_3C_2T_x$ MXene nanocomposites to NH_3 at room temperature. *J. Alloys Compd.* **2022**, *898*, 162812. [CrossRef]
77. Syrový, T.; Kuberský, P.; Sapurina, I.; Pretl, S.; Bober, P.; Syrová, L.; Hamáček, A.; Stejskal, J. Gravure-printed ammonia sensor based on organic polyaniline colloids. *Sens. Actuators B Chem.* **2016**, *225*, 510–516. [CrossRef]
78. Bandgar, D.K.; Navale, S.T.; Nalage, S.R.; Mane, R.S.; Stadler, F.J.; Aswal, D.K.; Gupta, S.K.; Patil, V.B. Simple and low-temperature polyaniline-based flexible ammonia sensor: A step towards laboratory synthesis to economical device design. *J. Mater. Chem. C* **2015**, *3*, 9461–9468. [CrossRef]
79. Li, X.; Xu, J.; Jiang, Y.; He, Z.; Liu, B.; Xie, H.; Li, H.; Li, Z.; Wang, Y.; Tai, H. Toward agricultural ammonia volatilization monitoring: A flexible polyaniline/$Ti_3C_2T_x$ hybrid sensitive films based gas sensor. *Sens. Actuators B Chem.* **2020**, *316*, 128144. [CrossRef]
80. Wen, X.; Cai, Y.; Nie, X.; Xiong, J.; Wang, Y.; Song, H.; Li, Z.; Shen, Y.; Li, C. PSS-doped PANI nanoparticle/$Ti_3C_2T_x$ composites for conductometric flexible ammonia gas sensors operated at room temperature. *Sens. Actuators B Chem.* **2023**, *374*, 132788. [CrossRef]
81. Wu, J.; Zhang, Q.E.; Zhou, A.A.; Huang, Z.; Bai, H.; Li, L. Phase-separated polyaniline/graphene composite electrodes for high-rate electrochemical supercapacitors. *Adv. Mater.* **2016**, *28*, 10211–10216. [CrossRef]
82. Yang, R.; Zhang, J.; Liu, J.; Li, G.; Qiao, Y.; Zhang, X.; Gao, J.; Lu, H. PANI/$Ti_3C_2T_x$ composite nanofiber-based flexible conductometric sensor for the detection of NH_3 at room temperature. *Sens. Actuators B Chem.* **2023**, *392*, 134128. [CrossRef]

83. Rather, M.H.; Mir, F.A.; Ullah, F.; Bhat, M.A.; Najar, F.A.; Shakeel, G.; Shah, A.H. Polyaniline nanoparticles: A study on its structural, optical, electrochemical properties along with some possible device applications. *Synth. Met.* **2022**, *290*, 117152. [CrossRef]
84. Rojas, R.; Pinto, N.J. Using electrospinning for the fabrication of rapid response gas sensors based on conducting polymer nanowires. *IEEE Sens. J.* **2008**, *8*, 951–953. [CrossRef]
85. Ahmed, F.E.; Lalia, B.S.; Hashaikeh, R. A review on electrospinning for membrane fabrication: Challenges and applications. *Desalination* **2015**, *356*, 15–30. [CrossRef]
86. Xue, J.; Wu, T.; Dai, Y.; Xia, Y. Electrospinning and electrospun nanofibers: Methods, materials, and applications. *Chem. Rev.* **2019**, *119*, 5298–5415. [CrossRef]
87. Zhang, Y.; Kim, J.J.; Chen, D.; Tuller, H.L.; Rutledge, G.C. Electrospun polyaniline fibers as highly sensitive room temperature chemiresistive sensors for ammonia and nitrogen dioxide gases. *Adv. Funct. Mater.* **2014**, *24*, 4005–4014. [CrossRef]
88. Kim, D.; Lee, J.; Park, M.K.; Ko, S.H. Recent developments in wearable breath sensors for healthcare monitoring. *Commun. Mater.* **2024**, *5*, 41. [CrossRef]
89. Sun, B.; Ding, Y.; Wang, Q.; Song, P. Rational design of 1D/2D heterostructured $ZnSnO_3$/ZnO/$Ti_3C_2T_X$ MXene nanocomposites for enhanced acetone gas sensing performance. *Sens. Actuators B Chem.* **2024**, *409*, 135541. [CrossRef]
90. Gui, Y.; Zhang, W.; Liu, S.; Li, Y.; Yang, J.; Jin, G.; Huang, H.; Yang, P.; Gao, M. Self-driven sensing of acetylene powered by a triboelectric-electromagnetic hybrid generator. *Nano Energy* **2024**, *124*, 109498. [CrossRef]
91. Peng, H.; Yang, J.; Lin, C.; Qi, L.; Li, L.; Shi, K. Gas-sensitive performance of metal-organic framework-derived CuO NPs/$Ti_3C_2T_X$ MXene heterostructures for efficient NO_2 detection at room temperature. *J. Alloys Compd.* **2024**, *980*, 173657. [CrossRef]
92. Seekaew, Y.; Lokavee, S.; Phokharatkul, D.; Wisitsoraat, A.; Kerdcharoen, T.; Wongchoosuk, C. Low-cost and flexible printed graphene–PEDOT:PSS gas sensor for ammonia detection. *Org. Electron.* **2014**, *15*, 2971–2981. [CrossRef]
93. Lin, Y.; Huang, L.; Chen, L.; Zhang, J.; Shen, L.; Chen, Q.; Shi, W. Fully gravure-printed NO_2 gas sensor on a polyimide foil using WO_3-PEDOT:PSS nanocomposites and Ag electrodes. *Sens. Actuators B Chem.* **2015**, *216*, 176–183. [CrossRef]
94. Jin, L.; Wu, C.; Wei, K.; He, L.; Gao, H.; Zhang, H.; Zhang, K.; Asiri, A.M.; Alamry, K.A.; Yang, L.; et al. Polymeric $Ti_3C_2T_x$ MXene composites for room temperature ammonia sensing. *ACS Appl. Nano Mater.* **2020**, *3*, 12071–12079. [CrossRef]
95. Atkare, S.; Kaushik, S.D.; Jagtap, S.; Rout, C.S. Room-temperature chemiresistive ammonia sensors based on 2D MXenes and their hybrids: Recent developments and future prospects. *Dalton Trans.* **2023**, *52*, 13831–13851. [CrossRef]
96. Qiu, J.; Xia, X.; Hu, Z.; Zhou, S.; Wang, Y.; Wang, Y.; Zhang, R.; Li, J.; Zhou, Y. Molecular ammonia sensing of PEDOT:PSS/nitrogen doped MXene Ti3C2Tx composite film at room temperature. *Nanotechnology* **2022**, *33*, 065501. [CrossRef]
97. Zhao, L.; Zheng, Y.; Wang, K.; Lv, C.; Wei, W.; Wang, L.; Han, W. Highly stable cross-linked cationic polyacrylamide/$Ti_3C_2T_x$ MXene nanocomposites for flexible ammonia-recognition devices. *Adv. Mater. Technol.* **2020**, *5*, 2000248. [CrossRef]
98. Chen, P.; Zhao, Z.; Shao, Z.; Tian, Y.; Li, B.; Huang, B.; Zhang, S.; Liu, C.; Shen, X. Highly selective NH_3 gas sensor based on polypyrrole/$Ti_3C_2T_x$ nanocomposites operating at room temperature. *J. Mater. Sci. Mater. Electron.* **2022**, *33*, 6168–6177. [CrossRef]
99. Zhou, J.; Hosseini Shokouh, S.H.; Komsa, H.-P.; Rieppo, L.; Cui, L.; Lv, Z.-P.; Kordas, K. MXene-polymer hybrid for high-performance gas sensor prepared by microwave-assisted in-situ intercalation. *Adv. Mater. Technol.* **2022**, *7*, 2101565. [CrossRef]
100. You, C.-W.; Fu, T.; Li, C.-B.; Song, X.; Tang, B.; Song, X.; Yang, Y.; Deng, Z.-P.; Wang, Y.-Z.; Song, F. A latent-fire-detecting olfactory system enabled by ultra-fast and sub-ppm ammonia-responsive $Ti_3C_2T_x$ MXene/MoS_2 sensors. *Adv. Funct. Mater.* **2022**, *32*, 2208131. [CrossRef]
101. Sardana, S.; Debnath, A.K.; Aswal, D.K.; Mahajan, A. WS_2 nanosheets decorated multi-layered MXene based chemiresistive sensor for efficient detection and discrimination of NH_3 and NO_2. *Sens. Actuators B Chem.* **2023**, *394*, 134352. [CrossRef]
102. Liu, Y.; Weiss, N.O.; Duan, X.; Cheng, H.-C.; Huang, Y.; Duan, X. Van der Waals heterostructures and devices. *Nat. Rev. Mater.* **2016**, *1*, 16042. [CrossRef]
103. Dey, A. Semiconductor metal oxide gas sensors: A review. *Mater. Sci. Eng. B* **2018**, *229*, 206–217. [CrossRef]
104. Wetchakun, K.; Samerjai, T.; Tamaekong, N.; Liewhiran, C.; Siriwong, C.; Kruefu, V.; Wisitsoraat, A.; Tuantranont, A.; Phanichphant, S. Semiconducting metal oxides as sensors for environmentally hazardous gases. *Sens. Actuators B Chem.* **2011**, *160*, 580–591. [CrossRef]
105. Lee, H.S.; Min, S.-W.; Chang, Y.-G.; Park, M.K.; Nam, T.; Kim, H.; Kim, J.H.; Ryu, S.; Im, S. MoS_2 nanosheet phototransistors with thickness-modulated optical energy gap. *Nano Lett.* **2012**, *12*, 3695–3700. [CrossRef]
106. Zhang, D.; Jiang, C.; Sun, Y. Room-temperature high-performance ammonia gas sensor based on layer-by-layer self-assembled molybdenum disulfide/zinc oxide nanocomposite film. *J. Alloys Compd.* **2017**, *698*, 476–483. [CrossRef]
107. Tang, M.; Zhang, D.; Wang, D.; Deng, J.; Kong, D.; Zhang, H. Performance prediction of 2D vertically stacked MoS_2-WS_2 heterostructures base on first-principles theory and Pearson correlation coefficient. *Appl. Surf. Sci.* **2022**, *596*, 153498. [CrossRef]
108. Zhang, X.; Wang, A.; Zhou, X.; Chen, F.; Fu, Q. Fabrication of aramid nanofiber-wrapped graphene fibers by coaxial spinning. *Carbon* **2020**, *165*, 340–348. [CrossRef]
109. Novoselov, K.S.; Mishchenko, A.; Carvalho, A.; Neto, A.H.C. 2D materials and van der Waals heterostructures. *Science* **2016**, *353*, aac9439. [CrossRef]
110. Hermawan, A.; Zhang, B.; Taufik, A.; Asakura, Y.; Hasegawa, T.; Zhu, J.; Shi, P.; Yin, S. CuO nanoparticles/$Ti_3C_2T_x$ MXene hybrid nanocomposites for detection of toluene gas. *ACS Appl. Nano Mater.* **2020**, *3*, 4755–4766. [CrossRef]

111. Song, Z.; Yan, J.; Lian, J.; Pu, W.; Jing, L.; Xu, H.; Li, H. Graphene oxide-loaded SnO_2 quantum wires with sub-4 nanometer diameters for low-temperature H_2S gas sensing. *ACS Appl. Nano Mater.* **2020**, *3*, 6385–6393. [CrossRef]
112. Yan, W.; Xu, H.; Ling, M.; Zhou, S.; Qiu, T.; Deng, Y.; Zhao, Z.; Zhang, E. MOF-derived porous hollow Co_3O_4@ZnO cages for high-performance MEMS trimethylamine sensors. *ACS Sens.* **2021**, *6*, 2613–2621. [CrossRef]
113. Lin, M.; Huang, Y.; Lei, Z.; Liu, N.; Huang, C.; Qi, F.; Zhao, N.; Zhou, Y.; Cao, J.; OuYang, X. UV-promoted NH_3 sensor based on $Ti_3C_2T_x/TiO_2$/ graphene sandwich structure with ultrasensitive RT sensing performances for human health detection. *Sens. Actuators B Chem.* **2024**, *410*, 135681. [CrossRef]
114. Yuxiang, Q.; Jing, X.; Yinan, B. Synergistic enhanced NH_3-sensing of SnS via $Ti_3C_2T_x$-oriented vertical growth and oxygen-containing functional group regulation. *Environ. Sci. Nano* **2022**, *9*, 1805–1818. [CrossRef]
115. Bhardwaj, R.; Hazra, A. MXene-based gas sensors. *J. Mater. Chem. C* **2021**, *9*, 15735–15754. [CrossRef]
116. Wang, X.; Li, Y.; Li, Z.; Zhang, S.; Deng, X.; Zhao, G.; Xu, X. Highly sensitive and low working temperature detection of trace triethylamine based on TiO_2 nanoparticles decorated CuO nanosheets sensors. *Sens. Actuators B Chem.* **2019**, *301*, 127019. [CrossRef]
117. Zhang, B.; Li, Y.; Luo, N.; Xu, X.; Sun, G.; Wang, Y.; Cao, J. $TiO_2/ZnCo_2O_4$ porous nanorods: Synthesis and temperature-dependent dual selectivity for sensing HCHO and TEA. *Sens. Actuators B Chem.* **2020**, *321*, 128461. [CrossRef]
118. Kim, S.J.; Koh, H.-J.; Ren, C.E.; Kwon, O.; Maleski, K.; Cho, S.-Y.; Anasori, B.; Kim, C.-K.; Choi, Y.-K.; Kim, J.; et al. Metallic $Ti_3C_2T_x$ MXene gas sensors with ultrahigh signal-to-noise ratio. *ACS Nano* **2018**, *12*, 986–993. [CrossRef]
119. Anasori, B.; Shi, C.; Moon, E.J.; Xie, Y.; Voigt, C.A.; Kent, P.R.C.; May, S.J.; Billinge, S.J.L.; Barsoum, M.W.; Gogotsi, Y. Control of electronic properties of 2D carbides (MXenes) by manipulating their transition metal layers. *Nanoscale Horiz.* **2016**, *1*, 227–234. [CrossRef]
120. Koh, H.-J.; Kim, S.J.; Maleski, K.; Cho, S.-Y.; Kim, Y.-J.; Ahn, C.W.; Gogotsi, Y.; Jung, H.-T. Enhanced selectivity of MXene gas sensors through metal ion intercalation: In situ X-ray diffraction study. *ACS Sens.* **2019**, *4*, 1365–1372. [CrossRef]